

Power Management, Monitoring & Control

SHARC Buoy Project



Prepared by:

Benjamin Connolly
CNNBEN002

Department of Electrical Engineering
University of Cape Town

Prepared for:

Robyn Verrinder

Department of Electrical Engineering
University of Cape Town

6 November 2022

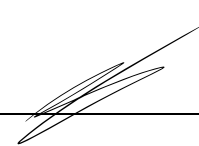
Submitted to the Department of Electrical Engineering at the University of Cape Town in partial fulfilment of the academic requirements for a Bachelor of Science degree in **Mechatronic Engineering**

Key Words: Power Monitoring; Power Control; Embedded Systems

Declaration

1. I know that plagiarism is wrong. Plagiarism is to use another's work and pretend that it is one's own.
2. I have used the IEEE convention for citation and referencing. Each contribution to, and quotation in, this final year project report from the work(s) of other people, has been attributed and has been cited and referenced.
3. This final year project report is my own work.
4. I have not allowed, and will not allow, anyone to copy my work with the intention of passing it off as their own work or part thereof.

Name: Benjamin Connolly

Signature: 

07 November
2022

Acknowledgements

I would firstly like to thank my supervisor, Miss Robyn Verrinder for all the support and guidance throughout this project, but also for trusting me to take the initiative and do the project to the best of my abilities. I would also like to extend a warm thank you to Mr Justin Pead for sharing his guidance and knowledge with me, and to Mr Brendon Daniels for assisting me with component requests and micro-soldering. Finally, a big thank you goes out to my parents for allowing me the opportunity to go to university and to be able to work on a project like this, as well as to my girlfriend, Lisa Bosman, and my friends who have done nothing but give me encouragement and support over the past months and weeks.

Abstract

It is a known fact that our earth is currently in one of the biggest climate change transitions. Antarctic sea ice is a useful indicator to determine what degree the climate has been changing as ice tends to melt as temperatures start to increase [1]. The Earth is heating up to temperatures which it has not reached previously. Since 69% of the world's fresh drinking water is trapped as ice in the Antarctic's ice sheets [3], there could be catastrophic consequences if this were to melt, as it could be lost in the ocean. Therefore, it is vital to develop systems to measure these ice changes through either satellite, or preferably in situ data collection. However, in situ measurements of Antarctic seasonal data have constantly been a problem for researchers. To resolve this possible issue, the UCT SHARC ice-tethered buoy is a novel, low-cost platform that will aid in the collection of these types of measurement data by being deployed in the Antarctic Marginal Ice Zone in the Southern Ocean.

The primary objective of this project was to create a power monitoring and control system which can be implemented in the UCT SHARC ice-tethered buoy. This system will interface and provide power to all the other subsystems on the buoy, which are integral to collecting in situ measurements from the area it is deployed in. The system will need to deal with a variety of operating modes, variations in loads and changes in efficiency due to the extreme weather. To assess these components, the (i) battery performance was evaluated, (ii) the previous power board was reviewed and (iii) the new power board design was analysed.

To evaluate the (i) battery performance, it was necessary to ensure that it can deliver the power it's rated to, as well as, seeing how the performance of the battery is affected by cold temperature. The battery evaluation experiment using hot and cold temperatures, was considered a success, as the hardware performed as expected and valuable data was gathered. From this experiment, it unfortunately was concluded that the battery packs perform much more poorly than what they were rated to do. The expected performance can be anticipated to be lower than the cold environment experiment results, due to the extreme temperatures found in the Antarctic.

The (ii) previous power board was assessed based on the current version of the power management, monitoring and control system for the buoy, thereby considering all design aspects of it. From the original board evaluation, several advantageous findings were made for example the input controls, capacitor bank, I2C Isolation and microcontroller. New changes were made to the board including using switching regulators, increasing the soft start time to 5s and adding a switch which can disconnect the capacitors whilst the microcontroller is being programmed.

From the power budget, battery evaluation, and evaluation of the original board, the (iii) next design of the power management, monitoring and control board was implemented. Modules such as the input control, soft start, I2C isolation, IO peripherals, temperature, ideal diode, and current increaser were deemed to work as expected and recommended to be used in future iterations of the board. The switching regulators worked effectively, but an investigation will need to be done to see as to why the MIC29302WU regulator wasn't functioning correctly. Many tests were unable to be done due to a programming pin error, while the new header pins and minor changes around the board made a positive impact on the usability of the board.

Overall, an effective power management system was thoroughly tested and described, and the power PCB improved upon, with recommendations made for future iterations.

Table of Contents

<i>Declaration</i>	<i>i</i>
<i>Acknowledgements</i>	<i>ii</i>
<i>Abstract</i>	<i>iii</i>
<i>Table of Contents</i>	<i>iv</i>
1. Introduction	1
1.1 Background to the study.....	1
1.2 Problem Statement	1
1.3 Project objectives	1
1.4 Scope and Limitations.....	2
1.5 Plan of development	2
2. Literature Review	3
2.1 Introduction.....	3
2.2 History of Antarctic ice data measurement	3
2.3 In situ Artic data collection platforms.....	6
2.4 Challenges of electronics operating in extreme environments	7
2.5 Power management	8
2.6 Batteries operating in cold environments.....	9
2.7 Current Limiting	10
3. Power Budget	11
3.1 Introduction.....	11
3.2 Methodology	11
3.3 Budget	12
3.4 Analysis	15
3.5 Conclusions	15
3.6 Recommendations	16
4. Battery Performance Evaluation	17
4.1 Introduction.....	17
4.2 Methodology	17
4.2.1 Constant Load Circuit Module.....	17
4.2.2 Feedback and Electrical Protection Module	23
4.2.3 Sensor Module	24
4.2.4 Microcontroller Module.....	24

4.2.5	Code.....	25
4.2.6	Implementation.....	27
4.3	Battery Evaluation Results	28
4.4	Discussion	29
4.5	Conclusions	30
4.6	Recommendations	31
5.	<i>Previous Power Board Evaluation</i>	32
5.1	Introduction.....	32
5.2	Breakdown and Understanding.....	32
5.2.1	Input Control Module.....	33
5.2.2	Current Monitoring Module.....	33
5.2.3	Regulator Module	34
5.2.4	Soft Start Module	34
5.2.5	Capacitor Bank Module	35
5.2.6	I2C Isolation Module	35
5.2.7	Microcontroller Unit Module	35
5.2.8	IO Peripherals Module	36
5.2.9	Temperature Module	36
5.2.10	Secondary Memory Module	36
5.2.11	Current Increaser Module	37
5.2.12	Ideal Diode Module	37
5.2.13	Test Points Module	37
5.3	Testing Methodology.....	38
5.3.1	Input Control Module.....	38
5.3.2	Regulator Module	38
5.3.3	Soft start	38
5.3.4	I2C Isolation.....	39
5.3.5	Ideal diode.....	39
5.3.6	Microcontroller	39
5.3.7	IO peripherals.....	40
5.3.8	Capacitor bank	40
5.3.9	Temperature	40
5.3.10	Current increaser	40
5.3.11	Secondary Memory & Current Monitoring	41
5.4	Results	42
5.5	Discussion	43
5.6	Conclusions	44
5.7	Recommendations	45
6.	<i>New Power Board Design</i>	46
6.1	Introduction.....	46
6.2	Design Methodology	46
6.2.1	Previous Design	46
6.2.2	Regulation Module	47

6.2.3	Soft Start Module	48
6.2.4	Test Points Module	49
6.2.5	Input Control Module.....	49
6.2.6	Microcontroller Module.....	50
6.2.7	Additional Changes.....	50
6.2.8	Implementation.....	50
6.3	Testing Methodology.....	51
6.3.1	Input Control Module.....	51
6.3.2	Regulator Module	51
6.3.3	Microcontroller Module.....	52
6.3.4	Soft Start Module	52
6.4	Results	52
6.5	Discussion	54
6.6	Conclusions	55
6.7	Recommendations	55
7.	<i>Conclusion.....</i>	57
8.	<i>List of References.....</i>	59
9.	<i>Appendix A.....</i>	63
10.	<i>Appendix B.....</i>	69
11.	<i>Appendix C.....</i>	74
12.	<i>Appendix D</i>	76
13.	<i>EBE Faculty: Assessment of Ethics in Research Projects.....</i>	77

1. Introduction

1.1 Background to the study

In situ measurements of Antarctic seasonal data have consistently been a problem for researchers. The UCT SHARC ice-tethered buoy is a novel, low-cost platform which will aid in the collection of in situ measurement data by being deployed in the Antarctic Marginal Ice Zone in the Southern Ocean. This project will specifically be focusing on the power management and control system section of the buoy and is instrumental in powering the buoy and allowing all the other subsystems to run.

1.2 Problem Statement

My vision for the project is to design, understand and implement an effective power management and control system for the UCT SHARC ice-tethered buoy that will aid in the collection of Antarctic in situ measurement data.

The primary sections of the project that need to be addressed are designing a power management and control model for the SHARC buoy which can effectively function in extremely cold weather and can perform for periods of up to 6 months at a time. Previous research and prototyping have gone into this project, but it has not been completely successful. I will be building upon and evaluating this information and prototyping with the aim of creating a more robust system which is able to achieve its goals. This is important because the SHARC buoy will not be able to function properly without a working power system. Thus, it will not be able to gather data, and will negatively affect every other subsystem on the SHARC buoy project.

1.3 Project objectives

The main objectives of this project are as follows:

- 1) Understand the requirements of the project
- 2) Conduct a literature review of previous work in this field and critically evaluate current technology/research
- 3) Produce a detailed power budget for the platform based on data sheets, project requirements and previous prototypes
- 4) Evaluate the current version of the power management system for the buoy, considering all design aspects.
- 5) Design a next iteration of the power system for the buoy considering battery topology, operating conditions and temperature, mission duration, cost, and size constraints
- 6) Produce a printed circuit board design for the system
- 7) Simulate the system under a variety of operating conditions and through a series of experiments designed for this purpose
- 8) Test and evaluate the power supply system performance based on a performance metric

- 9) Discuss the performance of the system, draw conclusions, and make recommendations for future improvements

1.4 Scope and Limitations

The primary objective of this project is to create a power monitoring and control system that can be physically implemented in the UCT SHARC ice-tethered buoy. This system will interface and provide power to all the other subsystems on the buoy which is integral to collecting in situ measurements from the area it is deployed in. The system will need to deal with a variety of operating modes, variations in loads and changes in efficiency due to the extreme weather.

Five primary assumptions are made going forward. Firstly, this is a real-world problem, therefore the assumption is made that components are not ideal and therefore call for a robust design. Secondly, the assumption is made that once the power budget is created, it will not change. Thirdly, the system is operating in extreme temperatures, and it is assumed these components may not act as expected; therefore, experimentation will be done to gauge how these elements function in cold temperatures. Fourthly, and perhaps the most important, is the assumption the previous power board is not working and will need to be tested in an evaluation phase. Fifthly, the board will be designed based on the designated 7.2 V, 58 Ah Lithium Thionyl Chloride battery packs supplied.

The system will have numerous limitations and the design will need to consider various factors such as the battery topology, temperature, mission duration, cost, and size constraints.

1.5 Plan of development

The report is structured into 7 chapters and very closely follows the process that was taken during the course of this project.

Chapters 1 & 2 are the introduction and literature review. These give background to the project, what the aims are, any assumptions and limitations, and goes into researched analysis of academic papers relating to this report.

Chapter 3 highlights the course of action which was taken in coming up with a power budget for this project. It delves into the results, discussion, conclusions, and recommendations regarding the power budget.

Chapter 4 focuses on the power supply evaluation, which details the processes taken in evaluating the battery packs that power the UCT SHARC buoy, as well as the results, discussions, recommendations, and conclusions relating to this topic.

Chapter 5 details the process taken when evaluating the previous power board, how its systems work, how it was tested, where it failed those tests, where it passed those tests, and what can be done going forward with the new buoy.

Chapter 6 outlines the method in designing the latest version of the power PCB. It highlights the testing it went through, the discussion and draws conclusions for future recommendations.

Chapter 7 finalizes and finishes off the report before the References, Appendices and Addendums sections.

2. Literature Review

2.1 Introduction

It is a known fact that our earth is currently in one of the biggest climate change transitions. Antarctic sea ice is a useful indicator to determine what degree the climate has been changing as ice tends to melt as temperatures start to increase [1]. Just over a year ago, the highest temperature was recorded in the Antarctic region at a high of 18.3° Celcius [2]. This leads us to believe the Earth is heating up to temeratures which it has not reached previously. Since 69% of the world's fresh drinking water is trapped as ice in the Antarctic's ice sheets [3], there could be catastrophic consequences if this were to melt, as it could be lost in the ocean. It has been estimated that sea levels may rise by 60 meters if this ice were to melt [4]. This highlights the importance of keeping attention on what the climate is doing on the Antarctic region, specifically focusing on how ice is forming and melting throughout the various seasonal cycles.

In the past, the primary methods of measuring ice levels and formations in the Antarctic regon have been with the use of satellites. These satellites have made use of microwave radiometer instruments which read microwave wavelengths [1]. Measurements can then be established to calculate brightness, temperature and imagery thereby developing sea ice maps [1]. Unfortunately, satellite measurements will never be as accurate as those done in situ due to issues with radar [5]. Additionally, in situ measurements are lacking in the Anarctic region due to the complex and often costly nature of these types of protocols, and are thus are needed by researchers for further tracking and study. Although this is the case, three diverse cost-saving ice tracking buoys, similar to the SHARC buoy, have been successful with data collection in the Arctic.

Additional problems such as freezing/refreezing of the ocean surface sheets in the marginal ice zone (MIZ) can prohibit the deployment of long-term buoys and thus measuring ice sheet data can be complex [6]. Commercial off-the-shelf (COTS) products which have been tested, stored, and theoretically, can perform under these harsh conditions [6], allows us to find cheaper and simpler components for projects such as the SHARC ice buoy. Each individual component of a buoy, however, must be tested as batch variation is an important factor to consider [6].

Specific components such as LDO regulators, which are major parts of the power management system, must also be considered and compared with other potential options as to make sure they are the correct choice for the SHARC buoy. We need to investigate the load the electronic systems are using, the overall capacity of the battery, type of battery and decide on a circuit which can protect against current spikes and keep the current within safe operating levels. This is done to understand the complexity, reliability, and robustness of a system, as a whole, which could potentially be used in extreme temperatures.

The aim of this project is to consider the several techniques of smart power management and control and to review its application and integration in the SHARC buoy for in situ Antarctic data collection in the sea in the Marginal Ice Zone.

2.2 History of Antarctic ice data measurement

Since December 1972, and still in use today, satellites have been used to measure the presence of sea ice in the Antarctic region [1][7]. The original Electrically-Scanning Microwave Radiometer (ESMR) was

utilized on the Nimbus-7 Defence Meteorological Satellite Program (DMSP) and SEASAT-A satellites before replacement by the Scanning Multichannel Microwave Radiometer (SMMR) in 1978 [8][9]. Both satellites use a dual polarized microwave radiometer with a five-frequency system which allows them to maintain a constant incidence angle with the earth; in so doing measuring predominantly weather data and ocean dynamics in polar regions [8][9]. Original findings included novel remapping of ice cover and anomalies on the perimeter of the Antarctic Sea ice pack [7].

A series of DMSP satellites using Special Sensor Microwave/Imager (SSM/I) instruments followed on from the SMMR tools in June 1987 [10][11]. The most modern of these is the DMSP satellites using the Special Sensor Microwave Image and Sounder (SSMIS) instrument which was created in October 2003 [10][1]. These types of satellites precision measure seven-channel microwave signals [12][13], are near-polar [14] and use the different properties of passive microwave signatures propagating off the surface of the Earth by different materials to determine what that material is (e.g. sea water vs ice) [1]. The enhanced use of microwave signals presented unique resources such as uniform polarizations, fixed spatial resolutions and common fields of view, over extended periods of time [10][11]. Through algorithm use, SSMIS instrument was also capable of determining ice edge and sea ice concentration, which were new measurements at the time of initiation [11]. Although breakthroughs were made with this new satellite technology, issues such as abnormally high reflector antenna emissions and solar illumination of the SSMIS warm calibration load caused issues with data retrieval [12].

One of the most modern approaches, aiming to make satellite ice information more accurate, is the use of the Gravimetry Satellites [3]. Developed by the National Aeronautics and Space Administration (NASA) and the German Research Centre for Geosciences (GFZ) in 2018, the Gravity Recovery and Climate Experiment Follow On (GRACE-FO) satellite was brought into existence [3]. These satellites work in pairs and rely on the principles of gravitational acceleration and how it affects their orbiting distance relative to one another, to calculate the mass of the surface below them [3]. If the satellites start orbiting at a fixed distance from one another, the general principle is the greater the increase in distance between the satellites over a fixed period, the greater the landmass over that same period (Figure 1). From this, scientists and engineers can decipher what type of material is below the satellite at a given time [3]. This allows much greater areas of the Antarctic to be covered at a given time, leading to a wider range of data becoming available [3].

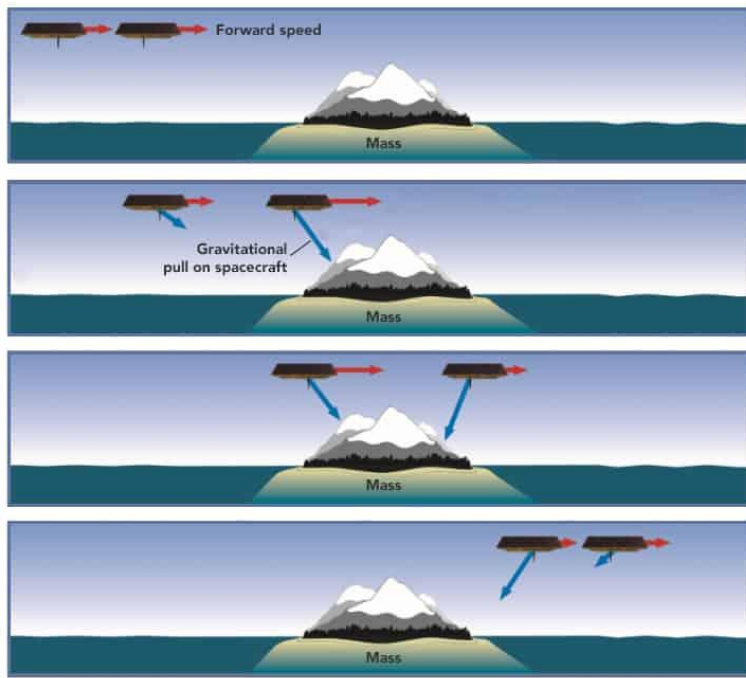


Figure 1 – An illustration showing how satellites can measure changes in ice and snow based on the gravitational pull of large masses on the Earth [3]

Another approach to increase the quality of data collected is by using data from multiple satellites and combining them to develop more accurate estimations of ice elevation changes [4]. These algorithms predominantly use data from satellites such as the European Space Agency CryoSat-2 [16] and the Global Monitoring for Environment and Security (GMES) Sentinel-3 [5] which are equipped with radar altimeters. Using data from two or more satellites, clustering algorithms are then applied to the data which rejects outliers and leads to an increase in the resolution of the data [4].

Between 2003 and 2011, the volume of ice in the Arctic recorded by CryoSat-2 was shown to have reduced by 1479 km^3 in winter and 4291 km^3 in autumn [16]. This is a major decline of ice formations due to greenhouse gases [16]. Based on data collected by CryoSat-2, there is a predicted decline of 3.4% of sea ice per decade [16], further demonstrating the necessity for meticulous and efficient ice monitoring devices worldwide. It has been noted that CryoSat-2 does however have its inefficiencies. These include biases such as whether the radar infiltrates completely through snow-ice interfaces and hence errors related to ice thickness and densities [16][17]. Similar to the CryoSat-2, the Sentinel-3A and Sentinel-3B satellites survey various locations on Earth in tandem, producing high-quality ice sheet and sea ice measurements [5][18]. The two satellites work in tandem within a 30s-time difference from one another on the same orbit, to ensure consistent data measurement and provision [18]. This also allows for thorough statistical analyses and almost repeat measurements [18]. As with CryoSat-2, sea ice dynamics, thickness, edge, type, and concentration are all researched to a high-resolution, and each satellite has a 7-year operational lifespan, allowing for continuous relays of information for scientists and policy makers alike [5].

Even though these advances have been made, these results are not as accurate as in situ data collection and are constantly being validated by researchers in the field [1]. Another point of concern with these sources of data, is that they do not take into account the factors experienced near the surface of the Earth that affect variations in ice, such as, oceanic and atmospheric circulations, as well as sea and air

temperatures [1]. These in situ measurements are lacking in the Antarctic region and are needed by researchers for further tracking and study.

2.3 In situ Artic data collection platforms

Ice sheet measurements are vital in situ techniques for monitoring ice patterns worldwide. Since 1989, over 150 different assessments of ice loss in Antarctica have been studied [19]. The initial in situ measurement systems were called ice mass balance (IMB) buoys and were designed for marine conditions [20]. These were created by the Cold Regions Research and Engineering Laboratory (CRREL) and the Scottish Association for Marine Science (SAMS) [20]. The original buoys were unfortunately large, complex, had many wires (which could be impacted by cold and water) and were difficult to deploy [20]. Consequently, autonomous monitoring systems were proposed in recent years.

Autonomous monitoring systems such as the one proposed by [20] uses remote sensing methods for in situ continuous measurements which are ideal as they are efficient, precise and have a high spatial resolution. They can last a couple of months and are easily deployed and transported to remote locations [20]. This specific model (the autonomous system for lake ice monitoring – ASLIM), measures vertical temperature distributions within sub-ice water and ice cover layers using short-wave radiation [20]. Although this is a lake monitoring system, its measuring methods for ice are useful references for other approaches and protocols, and potential buoys.

To provide a platform for this project, current buoy-based technologies that are similar in operation and environmental capacity should be analysed. Buoys currently being used in the Arctic and Antarctic regions are similar to the SHARC buoy in their in-situ data collection as well as being depolyed in icy, sub-zero sea environments. Three buoys that are of particular interest are the Seasonal Ice Mass Balance buoy version 3 (SIMB3) [21], the open source ice instrument (OSIC) [22], and the NOAA Pacific Marine Environmental Laboratory (PMEL) ice collection buoy [23] as all of these buoys have been built and deployed in the Northern polar region.

In 2011, the SIMB3 was developed to collect data on seasonal ice [20]. Initial SIMB designs were complex and expensive as well as labour intense and thus a cheaper, more resilient and comprehensive device was developed [24]. The newer SIMB3, would float and gather data as ice floes built up around it and melted with time [21]. This buoy had reduced instrument size and weight compared to previous SIMB's [20]. It was also built using off of shelf components and thus was created to be low cost [21], which is in line with the SHARC buoy's requirements. The SIMB3 records ice positions on the surface and bottom, air temperature and pressure, snow depth as well as GPS location [24]. Specifically looking at the battery system and power management system for the buoy, it makes use of a custom-made 18 V, 1620 Wh, alkaline battery pack [21]. The power management system of the buoy comprises of two LMZ12003TZ-ADJ/NOPB switching regulators which provide 3.3 V and 5 V outputs, respectively [21]. The use of an alkaline battery pack could theoretically be considered a poor design choice, due to a study done by a leading manufacturer of batteries [25], as alkaine-based batteries do not perform well under cold conditions and lose a significant amount of their electrical potential compared to Lithium-based batteries [25]. This is primarily due to the cold temperatures affecting the rate of reactions of the chemicals used in the battery cells [25]. Figure 2 visualises the affect of cold weather on alkaline-based batteries.

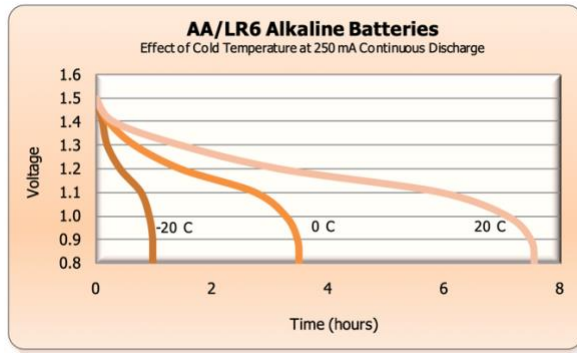


Figure 2 - Impact of temperature on alkaline battery performance [25]

The open source ice instrument (OSIC) was a buoy developed by researchers in Norway and Canada in 2018 to measure wave propagation in sea ice in the Arctic regions [22]. This isn't a floating buoy, but rather has a fixed land module with sensors that dip in the water level to collect data [22]. Specifically looking at the battery system and power management system, the device uses a LiFePO₄ battery cell, a solar panel, and a step-up converter. The LiFePO₄ battery has inherent advantages compared to other battery types such as its ability to withstand cold temperatures, its robustness [22], and its ability to be recharged. The power management module is basic in circuit design and consists of a U3V50F5 Pololu boost regulator to convert battery voltages to 5 V for the rest of the system. The ATMEGA328P microcontroller controls the power system, specifically the control of the charging system and optimising the power fed to the data logging system [22]. The design choice for the power management controller was deemed to be a useful choice as the ATMEGA328P is a low-power microcontroller [22] which is comparable in functionality to other microcontrollers such as the STM32 family.

The NOAA Pacific Marine Environmental Laboratory (PMEL) ice collection buoy was designed and tested in 2017 as a low-cost buoy to collect oceanographic data at water ice boundaries [26]. It operates in cryogenic temperatures [23], measuring data directly under the ice under the MIZ, which are crucial for understanding Antarctic ecosystems and ice shifts [26]. Due to these characteristics, it is similar with the SHARC buoy design requirements, as well as its autonomy. Unlike the SHARC buoy which uses a Lithium-based battery, this ice buoy is more similar to the SIMB3, as it uses a custom 9V, 28Ah alkaline pack [23]. As previously noted, this type of battery is theoretically unreliable based on evidence produced by [25].

Investigating the three devices provides insight to how buoys and data collection devices are designed for operation in cold, harsh, icy environments. It considers robust and low-cost tools devised by researchers from various countries with similar goals of comprehensive ice data research in mind.

2.4 Challenges of electronics operating in extreme environments

The Antarctic can reach temperatures of up to -60 Celsius [2]. Freezing and refreezing the ocean surface sheets in the marginal ice zone (MIZ) prohibits the deployment of long-term buoys. This can also affect many factors, such as sensor functionality and data-capturing capacities [27]. Therefore, measuring ice sheet data can be complex, specifically due to temperature "within military specification temperature range" (-55°C to 125°C) [6].

Fortunately, many commercial off-the-shelf (COTS) products have been tested, stored, and theoretically, can perform under these military specification conditions [6][28]. This allows us to find cheaper and simpler components for projects like this. Even though hypothetically, COTS products should work well in cold environments, certain products have reduced capacity from temperatures below -55 °C [29]. This lowers the reliability of the different parts [28][30]. In further experiments by [6] at -40 °C, it was found that this temperature seems to be the cut-off for most COTS parts regarding abnormal functionality. Although there are drawbacks, some COTS parts in colder temperatures have increased metal conductivity and memory maintenance [6], which could aid particular systems to have improved functionality.

Another unfortunate drawback of using COTS components is the considerable inter-batch variation between various batches and different manufacturers of the same product [6][29]. Extensive testing must then be done on specific components and between batches to ensure they are viable for extended periods of time in extreme conditions such as the Antarctic, yet this can be a costly process [6]. To try and mitigate this factor, systems consisting only of COTS components should be protected in a module that could protect the less robust parts from the cold [28][30]. This could improve system efficiency; however, it could also make the whole system more complex and have a heavier weight and larger size [30].

When considering the different elements of the original SHARC buoy design [27] within cryogenic temperatures, it is essential to evaluate the challenges experienced by some of the components, such as the voltage regulators, specifically the low drop out (LDO) voltage regulators, N-channel and P-channel MOSFETs, capacitors and resistors; as well as to determine which materials would be best suited for the various individual components. Voltage regulators, including LDOs, vary significantly under different test conditions due to electrical shifts, specifically any temperature under -40 °C [6]. N and P-channel MOSFETs, on the other hand, had optimistic results in extreme conditions, specifically regarding temperature [31]. In these same conditions, COTS resistors demonstrated less than 5% variational changes in resistance, which is useful for further investigation and use in a PCB board [6].

Polyester, polystyrene, polycarbonate, and tantalum capacitors have been proven to function effectively at low temperatures, while ceramic ones were seen to have poor capacity in cryogenic (-150 °C) temperatures [6]. Fortunately, as the lowest temperature recorded in the MIZ was -60 °C [2], hence this should not be an issue for the SHARC buoy.

2.5 Power management

One of the primary objectives of the power management system was to ensure that the voltage is regulated to a level where it is usable by other components on the board. Considering the type of application the SHARC buoy will be experiencing, linear LDO regulators or switching regulators are likely to be used.

LDO regulators can maintain a specific output voltage throughout various input voltages and load currents [32]. They are useful within printed circuit board (PCB) routing and to improve power efficiency within circuits by reducing noise and turning unnecessary functions off [32]. The key difference between an LDO regulator and a standard linear voltage regulator is the LDO can still regulate voltage, even when the difference between the input and output voltages is small [32]. This is an especially advantageous type of regulator for a system with a battery power source which does not have a significantly higher voltage than the voltage required by the equipment [32]. Considering the power management system will have a low-power requirement, a low-quiescent current LDO regulator should

be used. One significant pitfall of linear LDO regulators is their large power dissipation during operation [33]. This is primarily due to the internal makeup of the regulator and the internal transistor operating in the linear region [33]. Because of this, these regulators typically do not have very high-efficiency rates [32]. The efficiency of the regulation system can be improved by connecting the LDO to the voltage supplied by a switching regulator [32].

Since the 1960's switch-mode power supplies have gained traction and are much more prevalent in modern technology [33]. Unlike their linear counterparts, switching regulators are more complex, but more efficient in their regulation of voltage [33]. This comes with the condition that these types of regulators are typically more complex in design [33] which can be difficult to manage. Switch mode power supplies (SMPS) are also prone to noise and output voltage ripple [33]. Comparing the switching regulator to the LDO regulator; the LDO is typically less expensive, has lower ripples, and faster transient responses [33]. However, it will not be as efficient as the SMPS [33].

2.6 Batteries operating in cold environments

The power source which runs the SHARC buoy will be crucial in determining the success of this project. Significant factors which need to be taken into account are the load of the electronic systems supplied, the redundancy level required, and the overall capacity of the battery [34].

Theoretically alkaline-based batteries do not perform well under cold conditions and lose a significant amount of their electrical potential in these conditions, compared to Lithium-based batteries [25]. This is primarily due to the cold temperatures affecting the rate of reactions of the chemicals used in the battery cells [25]. Figure 2 visualises this effect as mentioned previously in the report. Alkaline-based batteries are not the only battery type which suffer performance issues in cold environments [35]. Experiments performed by [35] for hybrid electric vehicle batteries, prove lithium-ion batteries also perform better in warmer temperatures, similar to alkaline batteries. This is primarily due to the conductivity of the electrolyte decreasing with temperature and significant performance drops are associated with temperatures from 0° C and within negatives [35]. Figure 3 demonstrates the results of the hybrid electric vehicle battery experiments done by [35].

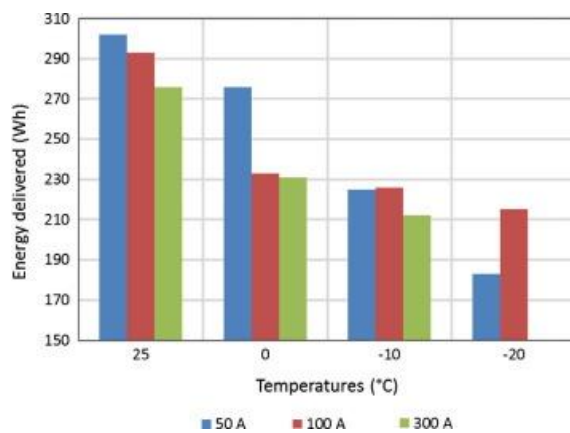


Figure 3 - Lithium Ion Experiment Test Results with Varying Temperature [35]

Considering cold temperature environments have significant effects on the performance of battery cells [25][35], the battery used for the SHARC buoy must be large enough to provide a sufficient quantity of power even after it experiences its capacity drop due to the cold [36]. Lithium Thionyl Chloride (LiSoCl₂) batteries are known for their high energy density [36]. LiSoCl₂ batteries are not only utilised for their

this factor, but also for their high voltage-producing characteristics and durability [36]. This makes them a worthy battery type for use in the SHARC buoy due to the extended length of time it will be based in the Antarctic as well as its robust qualities.

2.7 Current Limiting

When discussing a power management system, an essential component would be looking at the current flowing in the circuit to keep it within safe operating ranges [37]. [37] state this is an “essential feature” when implementing switching regulators. This is referred to as a ‘soft start’ system, and it is typically only used on start-up to mitigate the effects of an inrush current [37].

A simple example of this type of circuit, would be the SLVA soft start circuit [38]. The circuit was designed to mitigate the effects of the current caused by the voltage overshoot when linear LDO voltage regulators are enabled and to limit the inrush current during start-up [38].

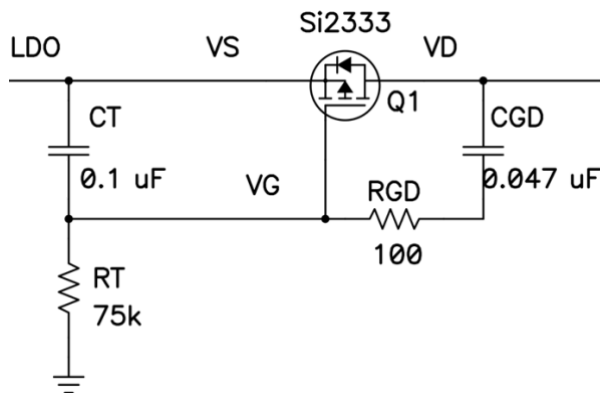


Figure 4 - SLVA156 Soft Start Circuit [38]

Important components RT and CT in Figure 4 control the soft start time; CGD must be must smaller than CT [38], as stated on the reference sheet.

The complexity of the soft start circuit ranges according to the circuit data sheet, and can be adapted for a range of applications such as industrial or light current systems. However, a basic soft start such as the one shown in Figure 4 is adequate for the level of design on the SHARC buoy.

3. Power Budget

3.1 Introduction

Considering that the SHARC buoy is made up of many different modules, the first steps in determining the specifications for the power management and control module are to determine what uses power, how it uses power, and how much power it uses.

The aim of this budget is to produce a list of equipment the SHARC buoy will be using, what power modes the different components have, as well as what power consumptions happen during those various mode cycles. This will be used to determine specifications for the power management and control module.

This will be achieved using component datasheets, as well as a database of modes and power requirements that had been compiled by previous researchers working on the SHARC buoy [39].

3.2 Methodology

The SHARC buoy was broken down into six major submodules:

- i. Inertial measurements module
- ii. Environmental measurements module
- iii. Processor module
- iv. GNSS module
- v. Communication module
- vi. Power management and control module

The primary components were investigated via information provided by their datasheets. Important material could be collected from this; mainly the voltage needed for that module, the processes that module would undergo in a cycle and how much current it consumed during those processes. The only submodule, which was not looked at, was the power submodule, as this budget was intended to derive specifications for it. The data was collected and processed using a Microsoft Excel spreadsheet.

The inertial measurements submodule consisted of a FXAS21002 gyroscope and a FXOS8700 accelerometer; both of which had 5 modes of operation. The environmental measurements submodule consisted of a DS18B20 temperature sensor which had 2 modes of operation. The processor submodule consisted of a STMF405QD microcontroller and had 5 modes of operation. For the microcontroller, it was assumed that it was running at 60 MHz, all peripherals were disabled, and that the ART accelerator was disabled. The GNSS module consisted of a NEO-7M-0-000 GLONASS, GNS, GPS receiver and had 7 modes of operation. The communication module consisted of a RockBLOCK 9603d Iridium module which had 6 modes of operation.

The durations for how long each device will remain in each mode of operation was then collected from the researchers involved in designing the different subsystems [39].

Most of this raw data had already been collected by previous researchers working on the SHARC buoy [39]. The process undertaken, was to curate data into a more readable format, modularize it, create graphs displaying key points, and to generate equations producing power summaries. Where data was missing, it was found by looking at datasheets for that specific component.

3.3 Budget

Table 1 demonstrates required voltage for the different submodules.

Submodule	Required Voltage (V)
Inertial Measurements	3.3
Environmental Measurements	3.3
Processor	3.3
GNSS	3.3
Communication	5

Table 1 - Submodule Voltage Requirements

Table 2 & 3, as well as, Figures 5, 6 & 7 show data relating to the inertial measurements' submodule.

Gyro Cycle (From Sandby to Active)						
Process	Time Start (s)	Average supply current (A)	Average power consumption (W)	Duration (s)	Peak current (A)	Time End (s)
Standby mode	0	0.0000028	0.000011088	0	0.0000028	0
Standby to ready	0	0.0027	0.010692	0.055	0.0027	0.055
Ready mode	0.055	0.0016	0.006336	0	0.0016	0.055
Ready to Active	0.055	0.0027	0.010692	0.308030303	0.0027	0.363030303
Active mode	0.363030303	0.0027	0.010692	0	0.0027	0.363030303

Table 2 - FXAS21002 Cycle Data

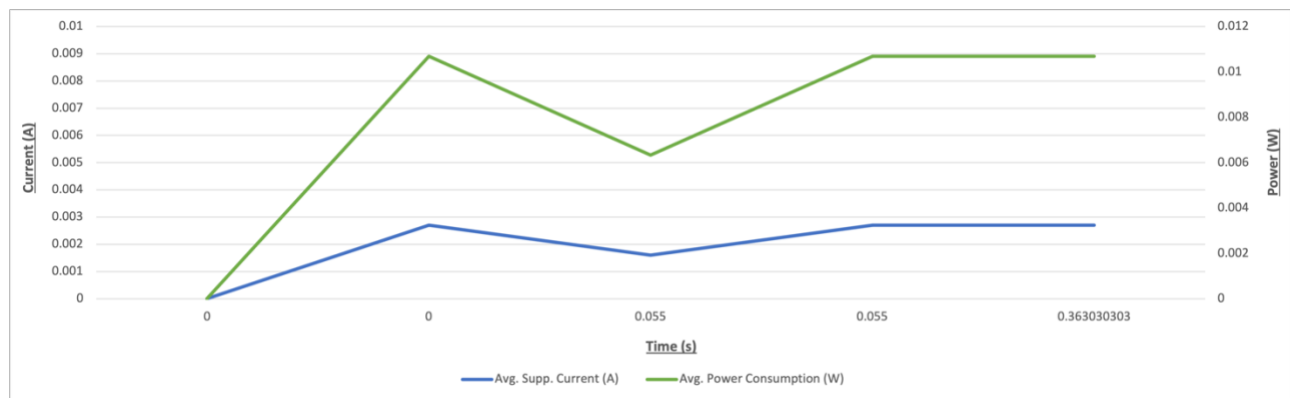


Figure 5 - FXAS21002 Power Consumption Graph Per Cycle

Accelerometer / Magnetometer Cycle (From Boot to Active)						
Process	Time Start (s)	Average supply current (A)	Average power consumption (W)	Duration (s)	Peak current (A)	Time End (s)
Boot sequence	0	0.000003	0.00001188	0.001	0.000003	0.001
Powered-down to active	0.001	0.00008	0.0003168	0.082	0.00008	0.083
Standby to active	0.083	0.00008	0.0003168	0.081	0.00008	0.164
Hybrid mode	0.164	0.00008	0.0003168	0	0.00008	0.164
Standby mode	0.164	0.000002	0.00000792	0	0.000002	0.164

Table 3 - FXOS8700 Cycle Data

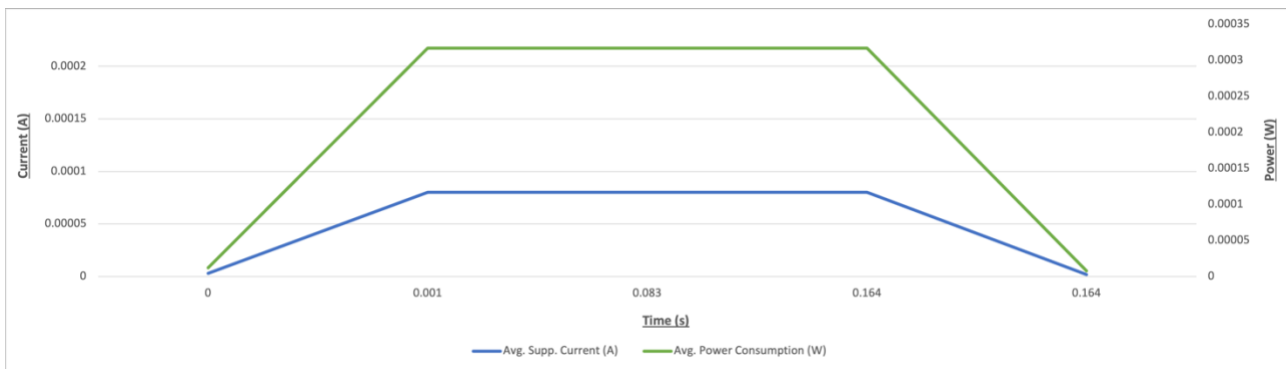


Figure 6 - FXOS8700 Power Consumption Per Cycle

Table 4 and Figure 7 relate to the environmental measurements submodule.

Temperature Sensor Cycle (From Standby to Active)						
Process	Time Start (s)	Average supply current (A)	Average power consumption (W)	Duration (s)	Peak current (A)	Time End (s)
Standby mode	0	0.000001	0.00000396	1	0.0015	1
Active mode	1	0.0015	0.00594	1	0.000001	2

Table 4 - DS18B20 Cycle Data

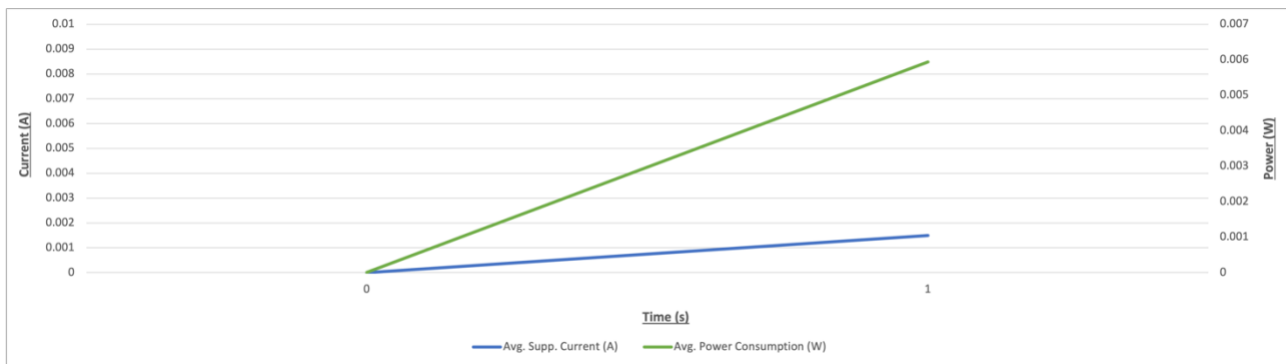


Figure 7 - DS18B20 Power Consumption Per Cycle

The following data (Table 5 and Figure 8) concerns the processor submodule.

Temperature Sensor Cycle (From Standby to Active)						
Process	Time Start (s)	Average supply current (A)	Average power consumption (W)	Duration (s)	Peak current (A)	Time End (s)
Standby mode	0	0.000001	0.00000396	1	0.0015	1
Active mode	1	0.0015	0.00594	1	0.000001	2

Table 5 - STMF405QD Cycle Data

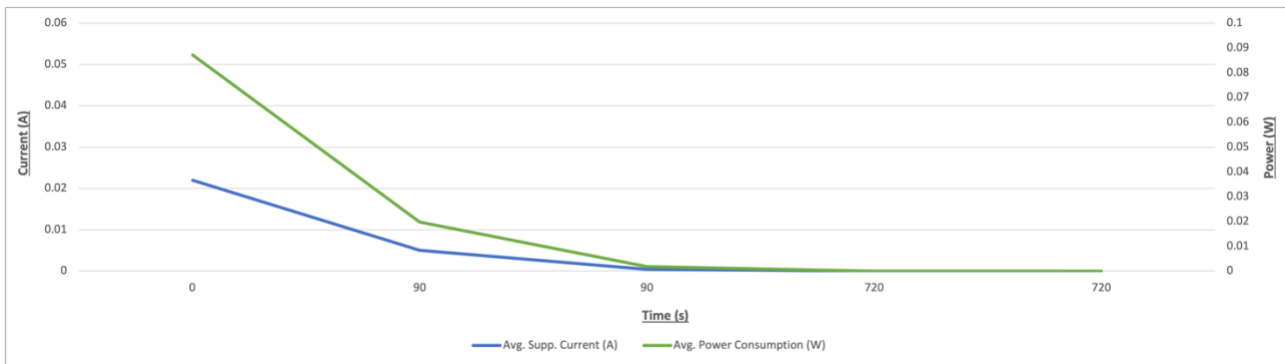


Figure 8 - STMF405QD Power Consumption Per Cycle

The GNSS submodule information is stated in Table 6 and Figure 9.

GPS Cycles (Start Cycles)						
Process	Time Start (s)	Average supply current (A)	Average power consumption (W)	Duration (s)	Peak current (A)	Time End (s)
Cold start (start)	0	0.022	0.08712	30	0.067	30
Cold start (end)	30	0.022	0.08712	0	0.067	30
Warm start (start)	0	0.022	0.08712	28	0.067	28
Warm start (end)	28	0.022	0.08712	0	0.067	28
Hot start (start)	0	0.022	0.08712	1	0.067	1
Hot start (end)	1	0.022	0.08712	0	0.067	1
Aided start (start)	0	0.022	0.08712	5	0.067	5
Aided start (end)	5	0.022	0.08712	0	0.067	5

Table 6 - NEO-7M-0-000 Start Cycles Data

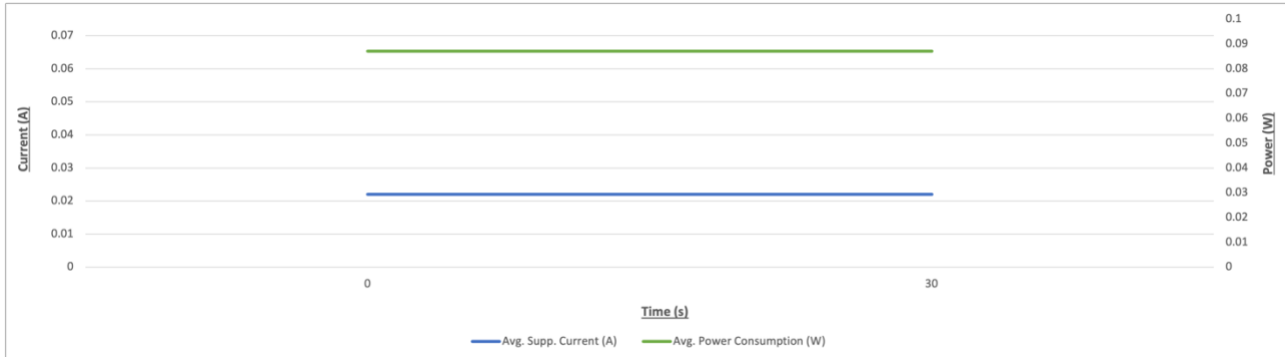


Figure 9 - NEO-7M-0-000 Power Consumption Per Cold Start Cycle

The Communications submodule data is found in Table 7 and Figure 10.

Communications Module Cycle (From Charge to Sleep)						
Process	Time Start (s)	Average supply current (A)	Average power consumption (W)	Duration (s)	Peak current (A)	Time End (s)
Charge	0	0.5	3	0	0.5	0
Idle	0	0.05	0.3	0	0.47	0
SBD success	0	0.05	0.3	60	0.47	60
SBD fail	60	0.065	0.39	60	0.47	120
Sleep transition	120	0.0001	0.0006	10200	0.0001	10320
Sleep steady	10320	0.00111	0.00666	3600	0.00111	13920

Table 7 - RockBLOCK 9603d Cycle Data

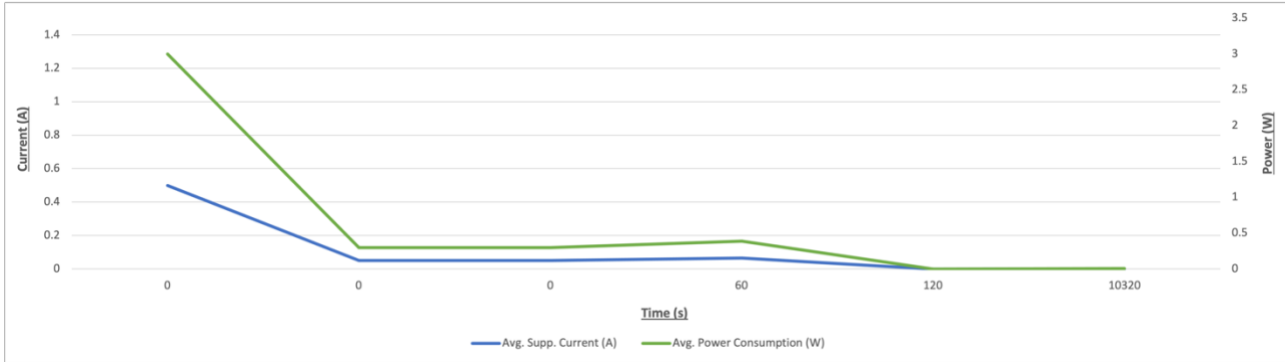


Figure 10 - RockBLOCK 9603d Power Consumption Per Cycle

A full version of this power budget can be found in Appendix A.

It is also important to note that the average power consumption column is calculated by multiplying the average supply current by the supply voltage and then further by a factor of 1.2 [39]. This additional factor was chosen by previous researchers as a buffer for more conservative power calculations [39]. Due to maintaining linearity in calculations, the power budget created for this report did not remove that 1.2 multiplication factor.

3.4 Analysis

Table 1 shows that all the equipment uses a 3.3 V and 5 V as the power source. Therefore, a specification for the power module is that it is able to regulate power from the 7.2 V battery voltage down to a useable 3.3 V and 5 V. Considering the battery voltage is not significantly higher than the required 5 V, a low-dropout voltage regulator may need to be used.

In Table 2-7, it is noted that the most power consumed is the by the RockBLOCK 9603d. The Iridium module draws a peak current of 470 mA at 5 V during most of its operation modes. This is significantly higher than the next highest power hungry component (the NEO-7M-0-000 receiver) which draws 67 mA at 3.3 V. Therefore, another specification for the power module, is it needs to supply a large amount of current (470 mA increase) when the Iridium module turns on.

The highest current drawn at a single moment can be calculated by adding the maximum peak currents for each of the devices from Tables 2-7. This came out to be 613 mA. Using a safety factor of 1.3 and rounding off, a specification for the power module is it needs to be able to handle a maximum of 800 mA of current passing through the module.

3.5 Conclusions

From the above results and analysis, we were able to draw 3 primary specifications for the power module. These were that the power management and control must:

- i. Be able to regulate the battery voltage to 3.3 V and 5 V
- ii. Be able to suddenly increase current supply 470 mA
- iii. Be able to handle a maximum current of 800 mA

3.6 Recommendations

One major recommendation suggested is in taking the power budget forward by creating a day-to-day schedule of which of the components mentioned in the power budget's methodology subchapter are in (i) what process state, (ii) when they are in that process state, and (iii) when they change from that state. This will allow for the power budget to be utilised more effectively in predicting how much power would be used, when it would be used, and could allow for optimising of the schedule as to maximise efficiency.

4. Battery Performance Evaluation

4.1 Introduction

In the scope and limitations section of the report, it is mentioned that we would not have any influence over the type of power source used and would adapt the design to whatever was provided. The power source for the buoy is a 72 V, 58 Ah, Lithium Thionyl Chloride battery pack which was custom made for this project.

The aim of this experiment is to evaluate the performance of the battery pack, to ensure that it can deliver the power that it's rated to, as well as, seeing how the performance of the battery is affected by cold temperature. This is an important test, as the project cannot run for the required period of 6 months if the batteries used are not delivering their rated power.

This will be done by subjecting the battery packs to constant load tests, in room temperature and cold temperature environments, and monitoring how the battery voltage fluctuates as a function of time. Referring to Figure 2 in the literature review, we are expecting the battery to follow a similar curve shape and have reduced performance in a colder environment. This would primarily be due to the decrease in the kinetic energy of the molecules and reduced rate of reactions, within the battery cells, involved in producing a voltage.

4.2 Methodology

4.2.1 Constant Load Circuit Module

i. Constant Current

The constant load circuit was the primary piece of hardware used and was designed to pull a constant current from its source, regardless of the voltage. This would simulate a load the source would be subjected to.

Firstly, the current that this device would need to draw needed to be calculated. Considering the rating of the battery pack is 58 Ah at 7.2 V and the buoy needs to last for a period of 6 months (183 days), the maximum daily power draw can be calculated:

$$P_{max} = \frac{58 * 7.2}{183} \quad [\text{EQT 1}]$$

$$P_{max} = 2.282 \text{ W per day} \quad [\text{EQT 2}]$$

Therefore, the maximum daily power that can be drawn from the batteries is 2.282 W which is the equivalent to 317 mAh at 7.2 V. Considering the load test of the battery packs will be on a much shorter time frame, it was decided to draw a similar current to the theoretical daily max, but instead each hour would represent a day. Therefore, the load circuit would draw a constant current of 350 mA, which can be used to calculate how long the batteries should theoretically last:

$$T = \frac{58}{0.35 * 24} \quad [\text{EQT 3}]$$

Therefore, when the batteries are subjected to a load that draws a constant 350 mA, the batteries should be drained within approximately 7 days. From the above calculations and the requirement for circuit to draw a constant 350 mA for the period of 1 week, the load circuit can be designed.

The design consists of an operational amplifier in a comparator configuration, which compares a control voltage to the output of the MOSFET. This is connected to the battery pack. As soon as the control voltage exceeds that of MOSFET output, the MOSFET is turned on and allows current to flow from the battery pack. This in turn increases current flowing through the circuit. This increases the reference voltage to a point in which the reference voltage exceeds that of the control voltage and the MOSFET is then turned off. The processes then repeats itself and this constant switching is done at a sufficient rate as to draw a constant current. The constant current can be controlled by the control voltage input to the op-amp. To draw a sufficient current, the battery current is dissipated through a $1\ \Omega$ resistor.

Additional resistors, R1 and R2, were placed at the output and inputs of the op-amp to limit current and a $10nF$ capacitor was placed between the output and the reference voltage input of the op-amp to counteract any ripple voltages which may occur. Additionally, a unity gain buffer was placed between the control signal and the comparator op-amp to increase the input impedance of the circuit.

The components selected for this design were the LM358 op-amp and the IRF540 MOSFET, as they met the specifications and were readily available from the White Lab store, which meant parts did not have to be ordered in. The resistors used were standard 1 Watt carbon-composition resistors. Since the current flowing through the $1\ \Omega$ resistor was high, $10 \times 10\ \Omega$ resistors would connect in parallel, to share the current equally between the resistors. This would more adequately distribute the current between all the resistors whilst achieving the same effect. Figure 11 displays the base design for the constant load circuit.

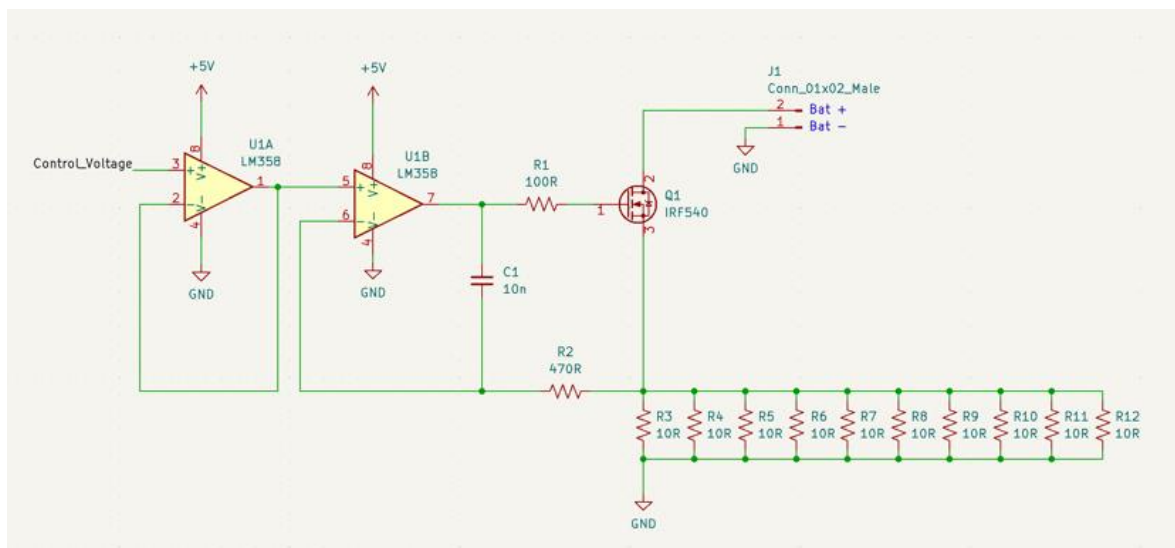


Figure 11 - Constant Load Circuit Base Design

ii. Control Voltage

A circuit to produce a control voltage to control the current in the load circuit was needed. Two methods were employed to achieve this. The first was using a standard $10\text{ k}\Omega$ potentiometer as a voltage divider. This allows the user to manually set the control voltage by turning a dial on the potentiometer. The second method was using a pulse width modulated (PWM) signal from a microcontroller, passed through a low-pass filter (LPF) to produce a voltage. By varying the duty cycle of the PWM signal, the average power produced would fluctuate and therefore, the average voltage would change too. This would permit the user to monitor the control voltage by adjusting the duty cycle of the PWM signal in software (assuming that the PWM signal is produced by a device that can be programmed).

When designing the LPF, a basic RC filter configuration was used and a response time of 5 ms was required. This would actively allow any sudden changes from the PWM signal to pass through the filter, whilst still filtering out the high frequency components. Deciding on a more robust design and having a conservative response time of 1ms in mind, the values for the resistor and capacitor for the filter were calculated as follows:

$$\tau = RC \quad [\text{EQT 5}]$$

Taking into account the E24 standard for selecting electronic components, the resistor was chosen to be $10\text{ K}\Omega$.

$$0.001 = 10000C \quad [\text{EQT 6}]$$

$$C = 100\text{ nF} \quad [\text{EQT 7}]$$

Therefore, the resistor was chosen be $10\text{ K}\Omega$ and the capacitor was calculated to be 100 nF .

The circuit was simulated in the LTspice Simulator to test the response of the filter before it was implemented into an real-world circuit. A Raspberry Pi Zero was used to produce the PWM signal and it has an amplitude of 3.3 V and a frequency of 8 KHz. The LTspice circuit would simulate a PWM signal with those same characteristics at the input to the filter. Figure 12 shows the LTSPICE implementation and results with a duty cycle of 50% are demonstrated in Figure 13.

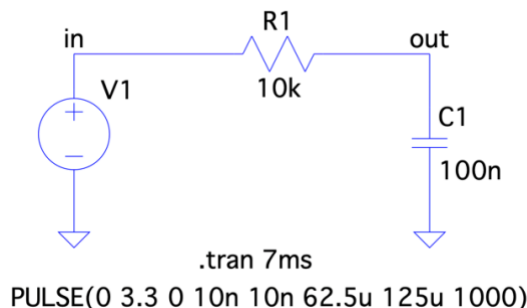


Figure 12 - LTspice First-Order Low Pass Filter Circuit

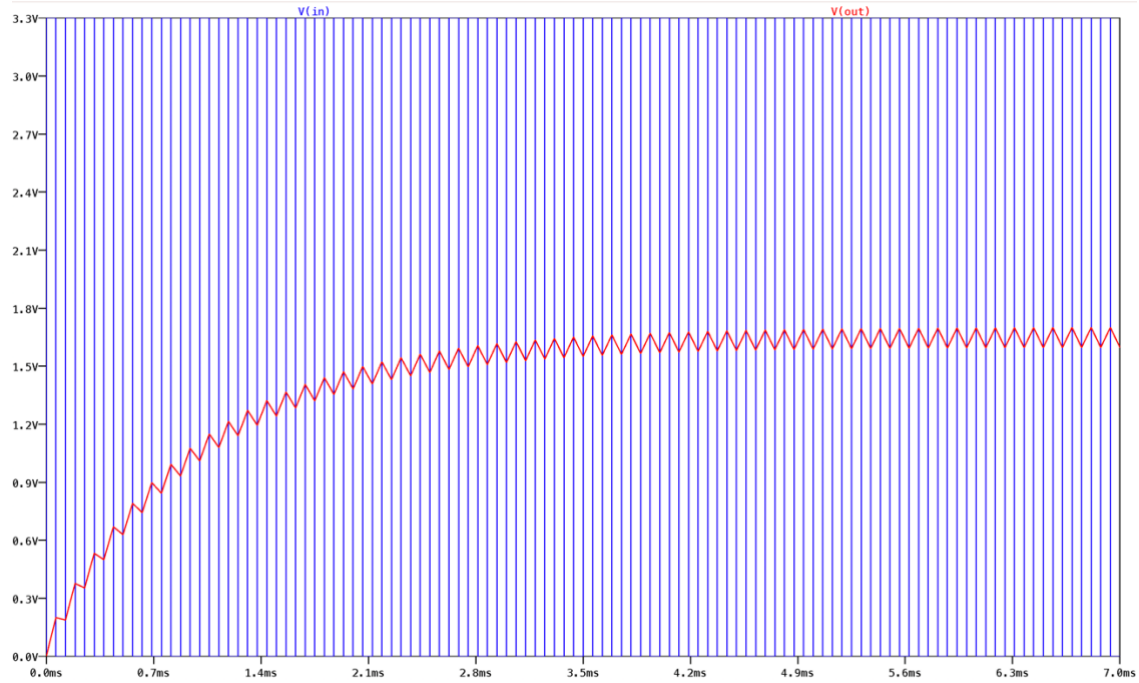


Figure 13 - LTspice First-Order Low Pass Filter Results

As seen from the results in Figure 13, the output voltage (red line) is jagged and is not as smooth as initially expected. The voltage ripple is too large and would cause the current in the load circuit to greatly vary. To solve this issue, a copy of the initial LPF was added onto the output of the LPF to create a second-order RC filter. Figure 14 shows the updated design for the LPF.

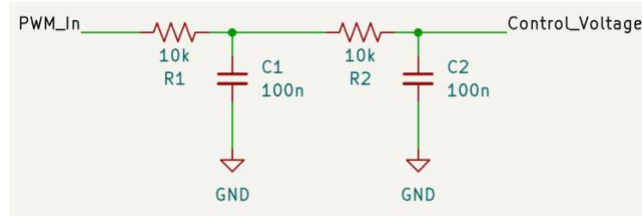


Figure 14 - Second-Order Low Pass Filter

The same conditions as the simulation in Figure 13, of 3.3 V and a frequency of 8 KHz, were used in the updated design LTspice simulation. Figure 15 illustrates the LTSPICE implementation and results of the updated design with a duty cycle of 50% are seen in Figure 16.

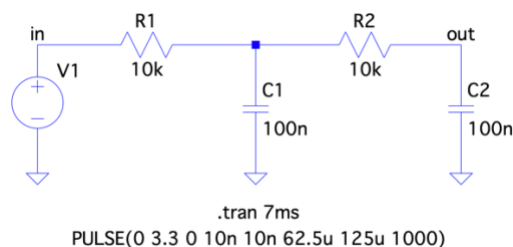


Figure 15 - LTspice Second-Order Low Pass Filter Circuit

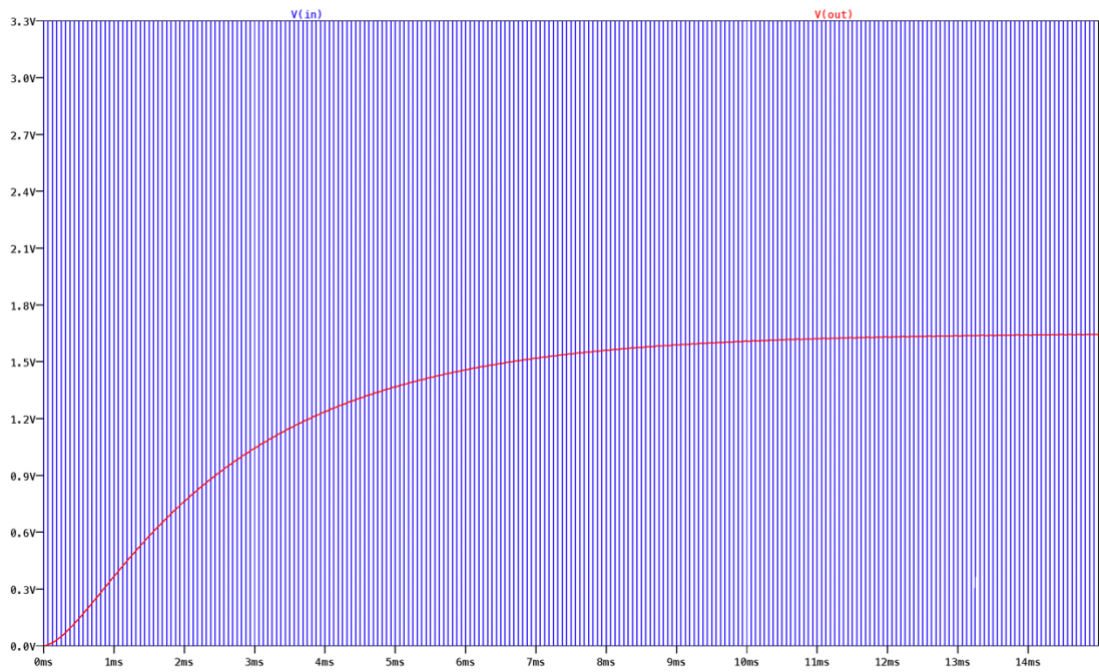


Figure 16 - LTspice Second-Order Low Pass Filter Results

The addition of the second stage to the filter, removed the ripples found in Figure 13 (Figure 16). However, it increased the response time to approximately 3 ms. This was deemed to still be adequate for the application, as it was within the required response time of 5ms. Figure 17 shows the output of the LPF for input PWM signals with a varying duty cycle.

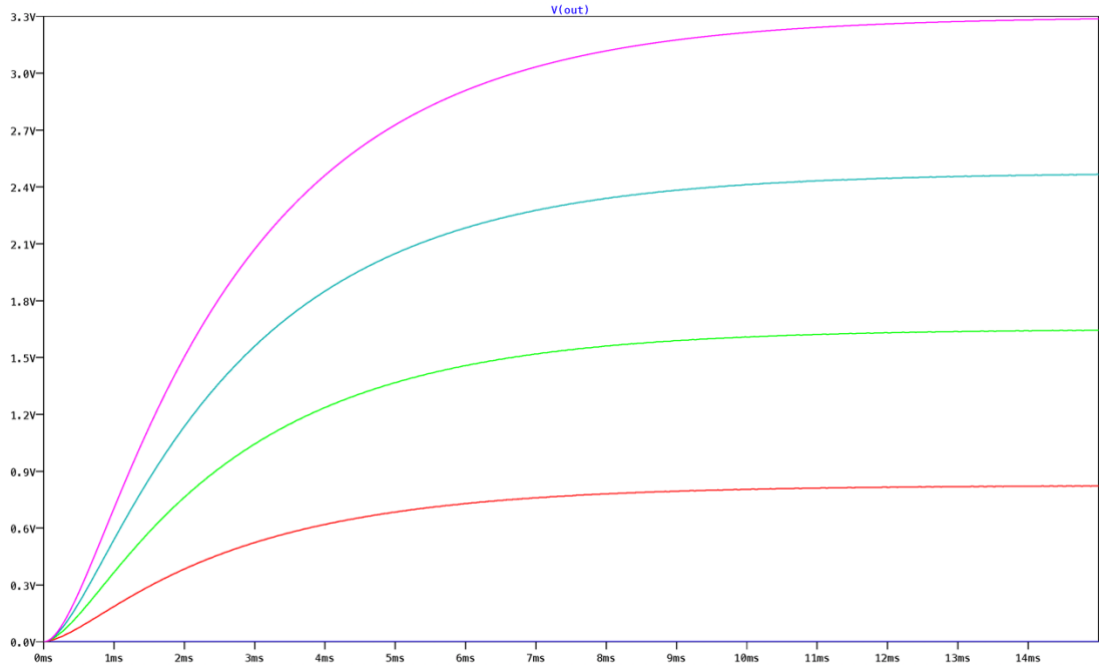


Figure 17 - LTspice Second-Order Low Pass Filter Varying Duty Cycle Results

The LPF (in simulation) can achieve the desired voltage output by changing the input PWM's duty cycle (Figure 17). These results were verified (Table 8) by implementing the LPF into a real-world circuit with a varying duty cycle and a pulse voltage from 0 V to 3.3 V to mimic the Raspberry Pi's PWM output.

<u>Duty Cycle (%)</u>	<u>Simulated Output Voltage (V)</u>	<u>Measured Output Voltage (V)</u>	<u>Ripple Voltage (mV)</u>
0	0.00	0.00	40
10	0.33	0.33	40
20	0.66	0.64	40
30	0.99	0.98	40
40	1.32	1.30	40
50	1.65	1.62	40
60	1.98	1.94	40
70	2.31	2.28	40
80	2.64	2.59	40
90	2.97	2.91	40
100	3.30	3.23	40

Table 8 - LPF Implementation Results

There is a slight deviation from the simulated results (Figure 17) compared to the measured real-world results (Table 8). This would most likely be due to power losses associated with the resistors and it was still deemed not to be an issue, as the output voltage can be controlled by changing the duty cycle of the PWM signal.

The designs of the potentiometer control and LPF control (Figure 14) could subsequently be merged into a single circuit (Figure 18). A switch was added to allow the user to determine if they would prefer to manually control the control voltage via the potentiometer or if they would prefer to use software to control the control voltage via the LPF and using PWM.

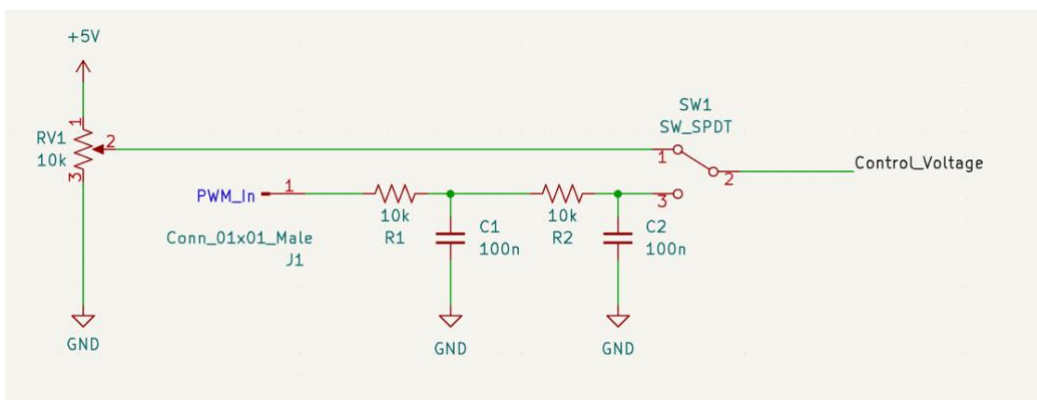


Figure 18 - Control Voltage Circuit

iii. Final Circuit

The above two circuits (Figure 14 and 18) were combined to form the constant load circuit used in the implementation of this experiment (Figure 19).

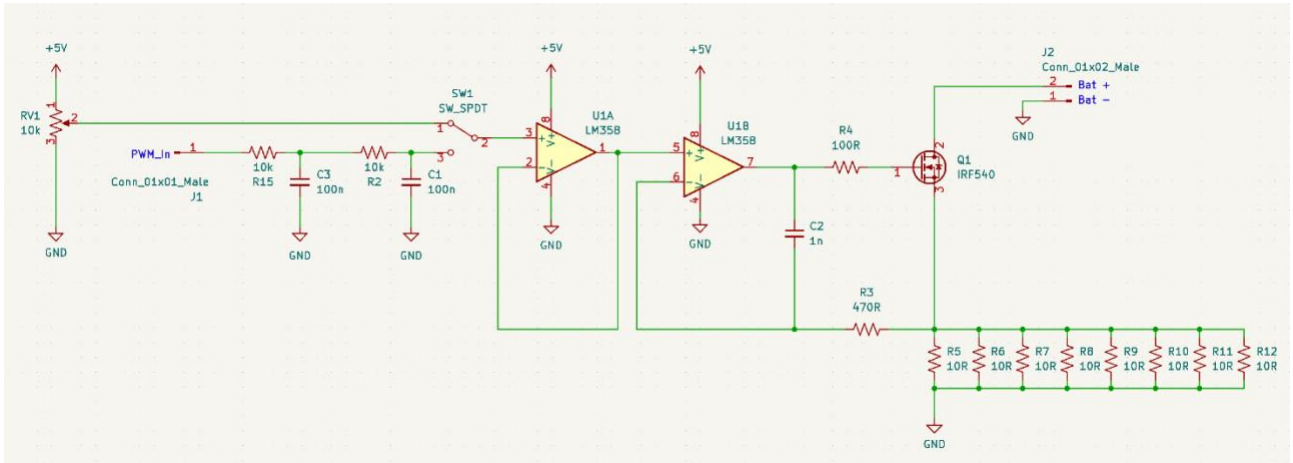


Figure 19 - Constant Load Circuit

This design was implemented into a real-world circuit and tested to ensure it functioned as it was designed to. Under controlled conditions, the circuit was powered by two voltage generators, one to act as a 7.2 V battery source and the other as the 5 V circuit power source. The circuit was tested using both the manual potentiometer control and the PWM control methods. This adequately allowed the circuit to draw a constant current anywhere from 0 A to 1A (voltage generator limit) and permitted the circuit to maintain that current, regardless of what the battery voltage was. All tests were passed.

It was noted, the IRF540 MOSFET got extremely hot during this test period. To combat the component overheating, a heatsink with thermal paste was added to the component to allow it to cool down more effectively.

4.2.2 Feedback and Electrical Protection Module

The feedback and electrical protection circuit (Figure 20) was designed to have 2 primary functions. The first being to provide feedback to the user via an array of LED's and a buzzer. This would let the user see how much current the batteries are drawing and to provide an alarm if the current exceeds its upper limit or if the load circuit gets too hot.

The second function was to provide electrical protection between the batteries and the load circuit and as a means to control that connection. This is done for two primary purposes. Firstly, it allows the batteries to only be connected to the load if the microcontroller is logging data. Secondly, and perhaps the most important, was to shut the circuit down in the event the microcontroller loses power. If this occurs, the control voltage will drop down to 0 V. In the event of the batteries being connected, it will cause the current drawn from the batteries to increase exponentially until it reaches the physical level at which the battery can discharge current. This will result in the components heating up to temperatures which irreparably damage the load circuit, battery pack and consequently, is a fire hazard. Power cuts are especially frequent in South Africa and the chances of the power failure during the 1 week experiment are high, therefore, the circuit will need this form of protection.

The feedback design makes use of a simple array of 3 LEDs; green for low current drawn, yellow for perfect current drawn, and red for high current drawn. A buzzer is included in the event the current drawn exceeds its upper limit (700 mA) as to alert the user. The electrical protection circuit acts as a breaker in between the battery and the load circuit and makes use of a relay switch to bridge the connection. This will permit the Raspberry Pi Zero to control if the circuit is bridged or not, via one of its GPIO pins.

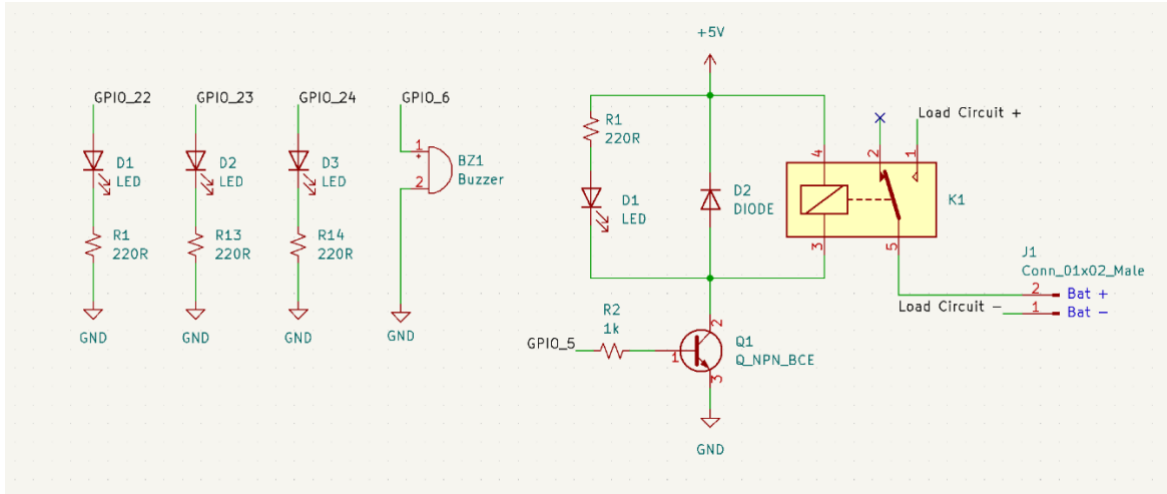


Figure 20 - Feedback and Electrical Protection Circuit

Under controlled conditions, the circuit was powered by two voltage generators, one to act as a 7.2 V battery source and the other as the 3.3 V Raspberry Pi GPIO output voltage. The buzzer and LEDs were individually tested to ensure they performed as expected. The relay output was measured to ensure that it read as 7.2 V when it was turned on and that it read 0 V when it was turned off. All tests were passed.

4.2.3 Sensor Module

The sensor circuit (Figure 21) is designed to capture data relating to the status of the battery. An INA219 sensor collects the battery's voltage, current, and power usage. This sensor uses the I2C communication protocol. An additional DHT22 sensor collects the temperature data and uses a custom 1-wire communication protocol developed by Adafruit Industries. This data collection was crucial in evaluating the battery pack.

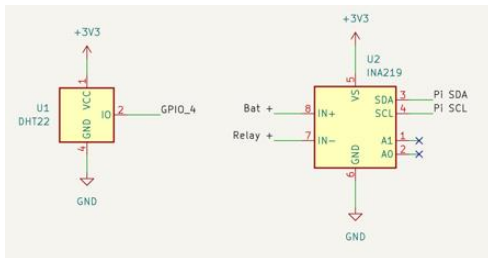


Figure 21 - Sensor Circuit

4.2.4 Microcontroller Module

The microcontroller used to run the experiment is the Raspberry Pi Zero W, as it provides an adequate amount of GPIO pins, can run python programmes, and could be accessed remotely. All data collected

during the experiment was stored on a 32 GB micro SD card inside the Pi. Figure 22 shows the schematic with the connections to the peripheral components.

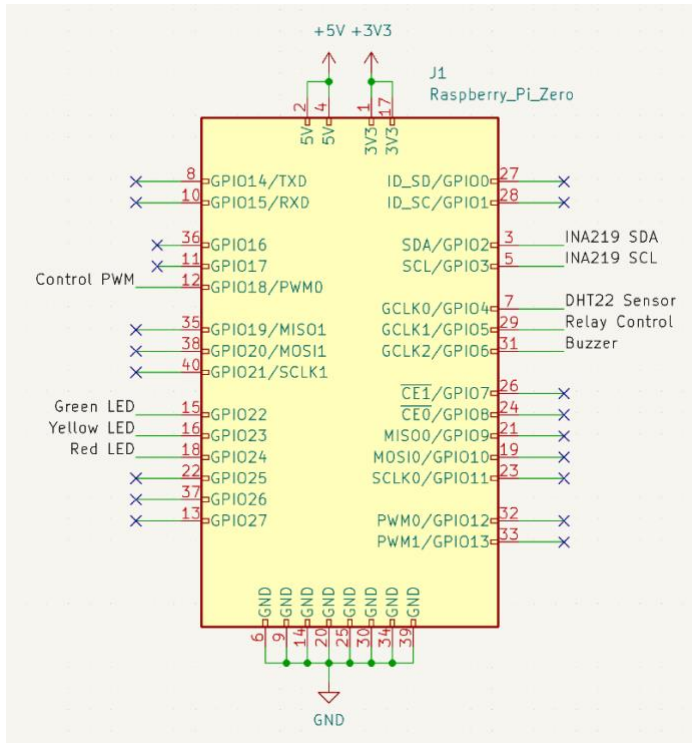


Figure 22 - Raspberry Pi Zero Peripheral Connections

4.2.5 Code

The software developed for this battery evaluation makes use of the hardware modules designed for this experiment. The primary goal of this software package was to be able to log the data coming in from the sensors, ensure that the hardware is running in a safe manner, and that the user had feedback to ensure that the hardware was running as expected.

A program was created to ensure that the software met its goals. The program was written in python and run on the Raspberry Pi Zero. The software consists of an initial setup stage where all variables and pins are initialised. The program then closes the relay switch and goes into an infinite loop which constantly reads in data, updates the PWM duty cycle and feedback peripherals, records a log of the data collected every 10 seconds and displays it to the terminal. If the current exceeds a limit of 700 mA (double that of the goal current for this evaluation experiment), the relay switch then opens, a buzzer sounds, and the program is shut down. If ^C is pressed, then the relay switch opens and the program is shut down.

The program was tested extensively, under controlled conditions, for every event which may occur and the outputs were monitored to ensure that the code behaved as expected.

Figure 23 outlines a flowchart the code follows.

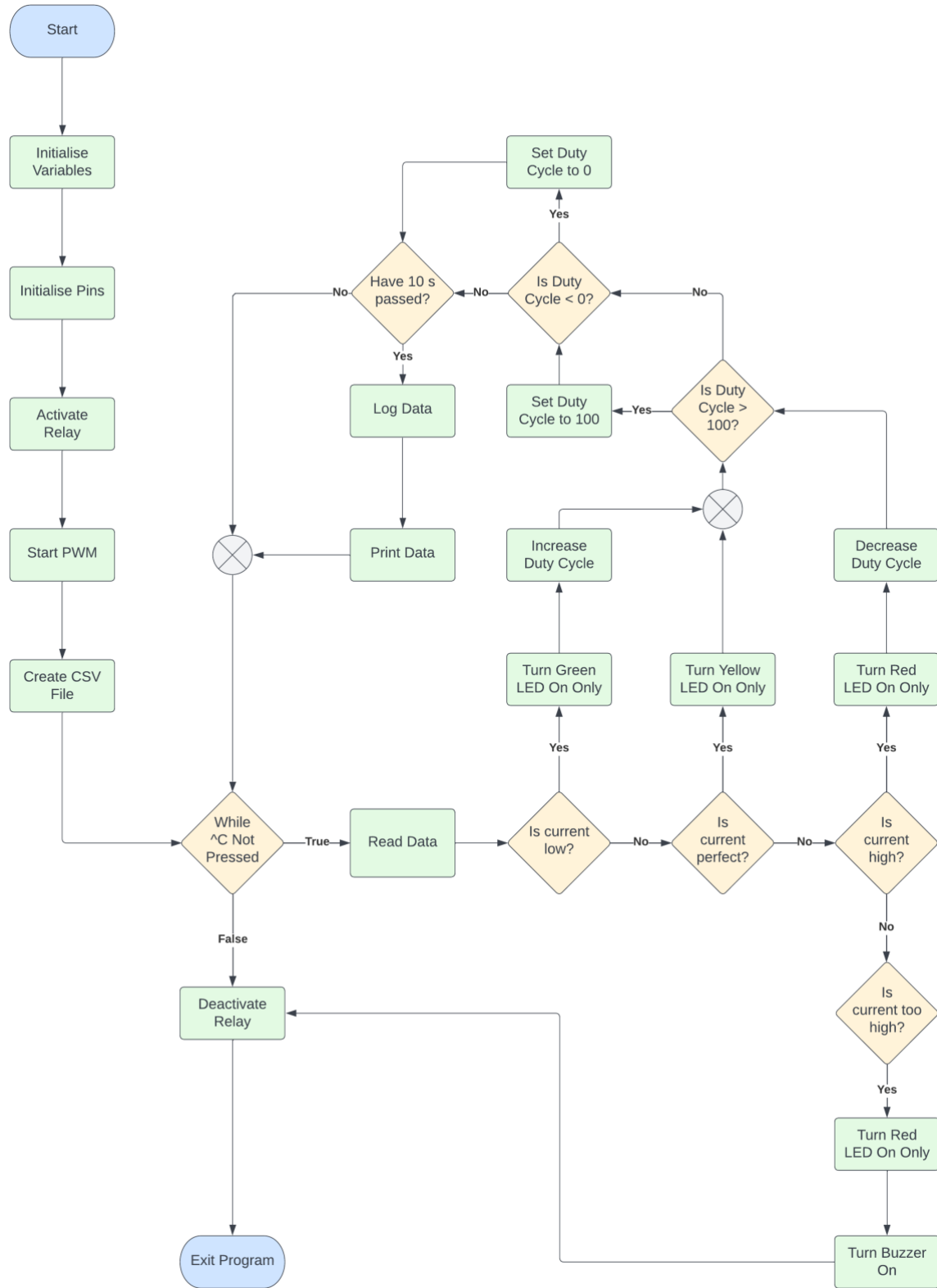


Figure 23 - Battery Evaluation Software Flowchart

A full copy of the python code developed for this battery evaluation can be found in Appendix B.

4.2.6 Implementation

The hardware described in the previous sections, needs to be able to coherently connect to one another to function effectively and test the battery pack. The different modules connect together as shown in Figure 24.

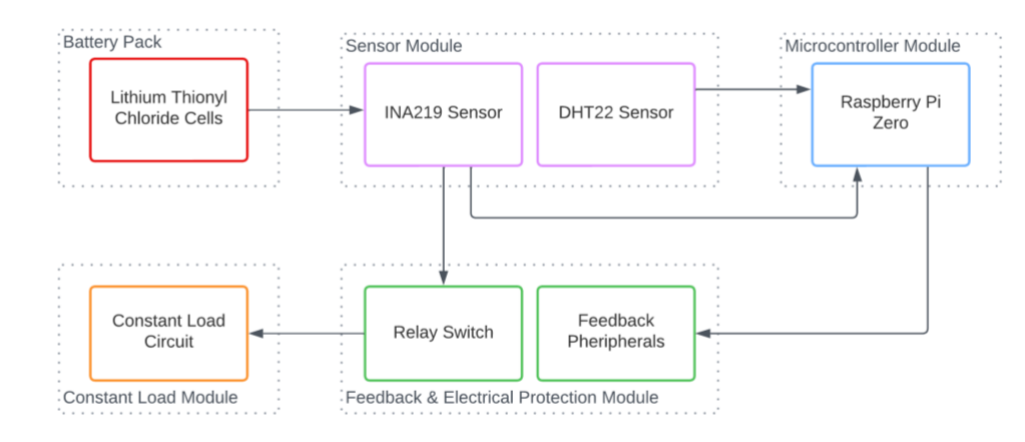


Figure 24 - Battery Evaluation Hardware Overview



Figure 25 - Battery Evaluation Hardware In Freezer

The steps for the evaluation experiment were initiated by connecting new battery packs with the hardware modules (Figure 24). The hardware was left in a household freezer for 24 hours (for a cold temperature experiment) (Figure 25) or at room temperature for 24 hours (for a warm environment experiment). This would allow the battery packs to sufficiently cool/heated to the temperature it was meant to be assessed at. The power was then turned on and the datalogger program started. If the manual control method was being used, the current for the load circuit was set as close as possible to 350mA. If the PWM control method was applied, the software would set the current correctly. This evaluation experiment made use of the PWM method of control. The current was monitored daily and adjusted to ensure that it stayed at a constant 350 mA and to ensure that the datalogger program was running. The current was then maintained until the voltage of the battery dropped to zero or if the battery could not supply any more current, which was approximately one week.

Due to power cuts over the weeks this evaluation experiment was run, the experiment unfortunately, was continually stopping and starting.

4.3 Battery Evaluation Results

For the battery test in a warm environment, the data logger logged 32826 unique data points which can be visualised in Figures 26 and 27.

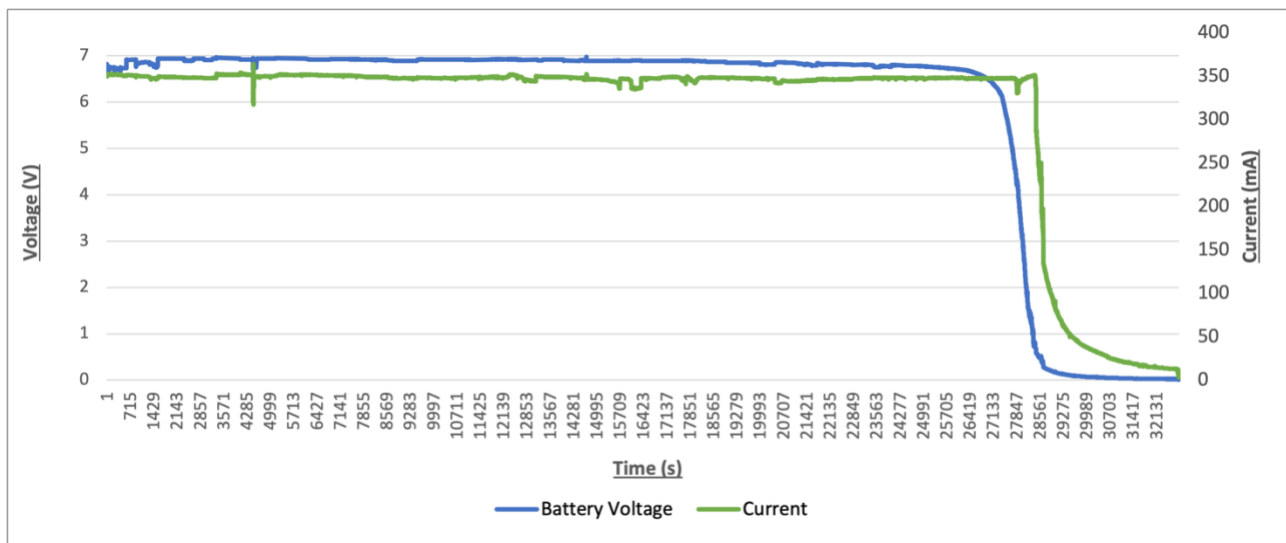


Figure 26 - Battery Voltage and Current In Warm Environment

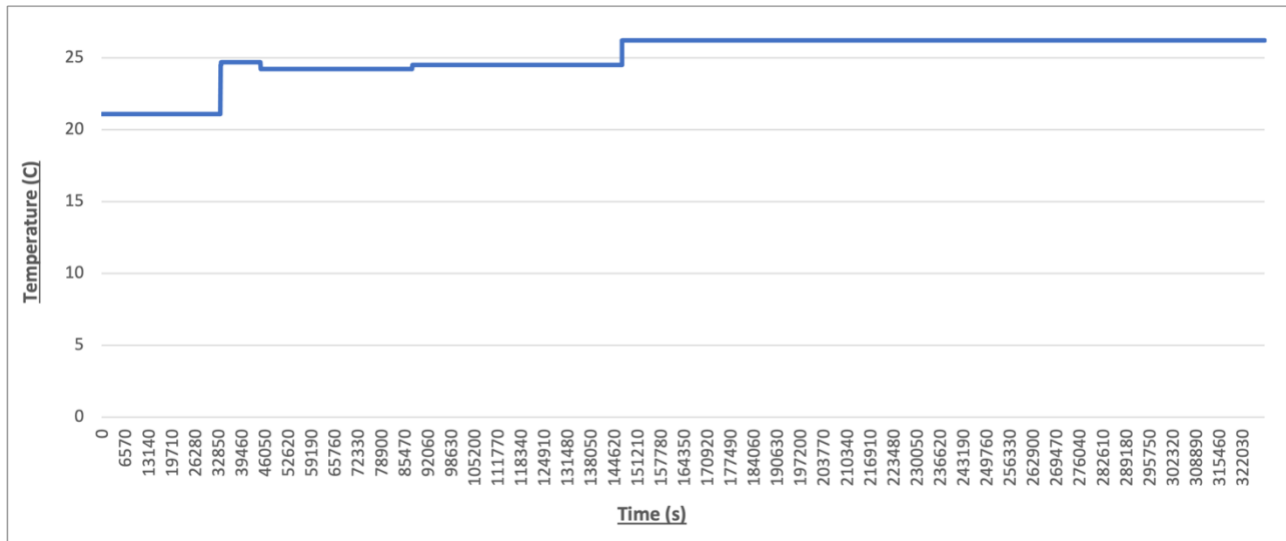


Figure 27 - Temperature For Warm Environment Battery Test

For the warm environment experiment, the average current test was 348 mA and the average temperature was 25° Celsius.

In a cold environment, the data logger logged 39954 unique data points which can be visualised in Figures 28 and 29.

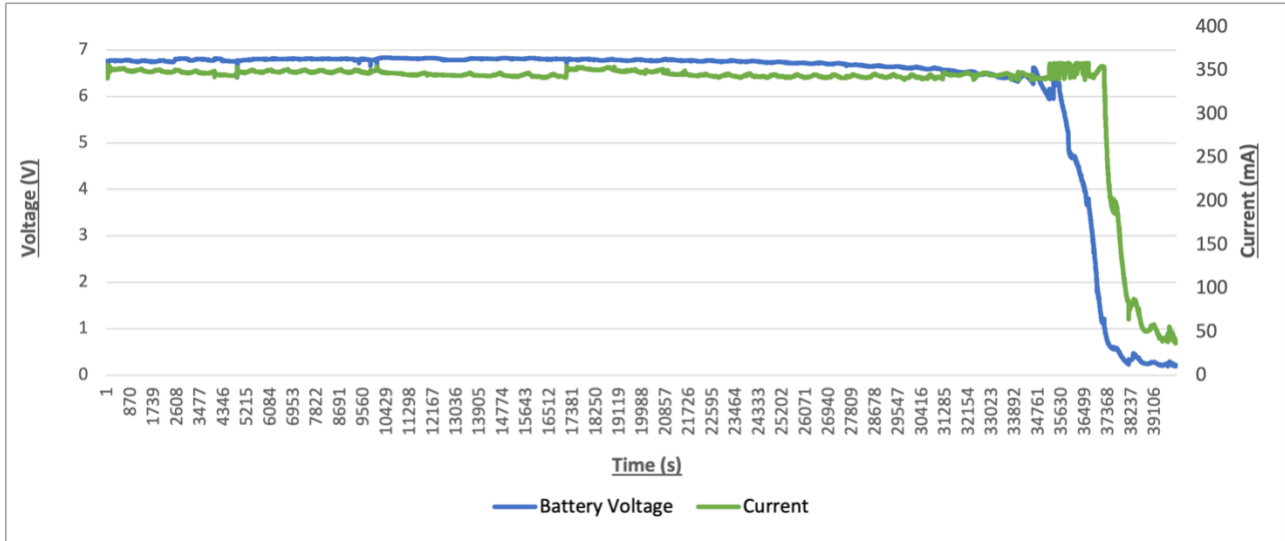


Figure 28 - Battery Voltage and Current In Cold Environment

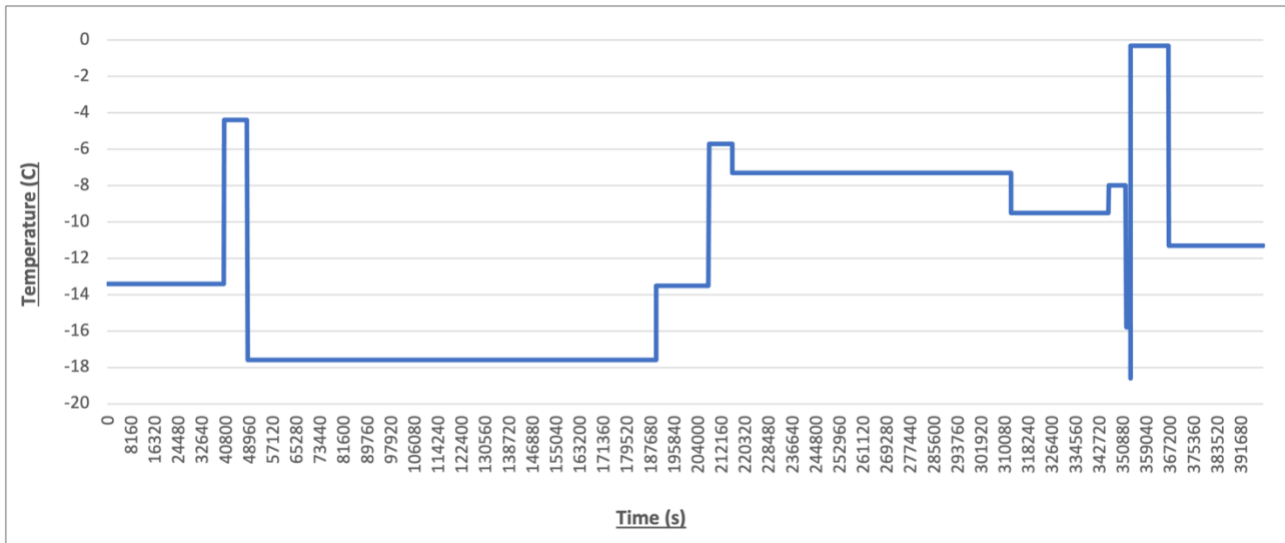


Figure 29 - Temperature For Cool Environment Battery Test

For the cold environment experiment, the average current test was 346. mA and the average temperature was -12° Celsius.

4.4 Discussion

The load testing circuit was able to pull a constant current of close to 350 mA, with minor fluctuations, for the duration of the experiment. This constant current was maintained until the batteries didn't have enough charge to supply a current and which caused the drop in the current (Figures 26 and 28) after the sudden drop in battery voltage. The minor fluctuations in Figure 26 and Figure 28 were most likely due to power cuts restarting the process, as well as the minor fluctuations in the control voltage. Additionally, the datalogger hardware logged data as expected.

In the warm environment experiment (Figure 26), the battery was able to supply a voltage of 6.9 V as soon as it was connected to the load circuit. This drop in voltage from 7.2 V would have been due to the

internal resistance of the battery cells. The battery pack supplied a constant average current of 348 mA for 284 550 seconds, and considering the average current, the Ah rating of the battery pack can be calculated:

$$Ah\ Rating = Avg.\ current * total\ seconds / 3600 \quad [EQT\ 8]$$

$$Ah\ Rating = 0.348 * \frac{284550}{3600} \quad [EQT\ 9]$$

$$Ah\ Rating = 27.5\ Ah \quad [EQT\ 10]$$

This is a concerning find, as it is not even 50% of the 58 Ah rating of the battery pack. Additionally, this battery pack tested in the warm environment should have lasted longer, compared to the battery pack tested in cold conditions. As discussed in the literature review section, this would primarily be due to the affected rate of reactions of the chemicals used in the battery cells [25].

In the cold environment experiment (Figure 28), the battery supplied a voltage of 6.8 V as soon as it was connected to the load circuit. As with the warm environment experiment, the 0.4 V drop in voltage would have been due to the internal resistance of the battery cells. This voltage drop was greater compared to the voltage drop of the battery pack tested in a warm environment, proving the colder environment affects the ability for the battery cells to produce electrical potential negatively.

The battery pack was able to supply a constant average current of 346 mA for 372 650 seconds, and considering the average current, the Ah rating of the battery pack can be calculated using the same method as EQT 8:

$$Ah\ Rating = 0.346 * \frac{372650}{3600} \quad [EQT\ 11]$$

$$Ah\ Rating = 35.8\ Ah \quad [EQT\ 12]$$

Although the Ah rating is better than the warm environment test, it is still only 61% of the of the battery pack. As it is known that battery cells perform poorer in colder environments, it is an expected and valid result.

It must be noted, the discharge curve is desirable as it is able to maintain an almost constant high voltage up until the end of its charge life, where it suddenly drops off (Figures 26 and 28). This is a favourable curve compared to one which starts to drop off slowly from the beginning to the end. Voltage regulators used on the power PCB board will need a voltage higher than 5 V to regulate down to 5 V, and 3.3 V, respectively. The discharge curve allows for this, as it provides a voltage higher than 6.5 V for most of its charge life.

4.5 Conclusions

The battery evaluation experiment can be considered a success, as the hardware performed as expected and valuable data was gathered. From this experiment, we can conclude the battery packs perform more poorly than what they were rated to do. This will need to be considered when coming up with a schedule to turn components on/off (outside the scope of this project, but relevant to the greater SHARC buoy project as a whole). Considering these battery packs will be subjected to an even colder environment than a home freezer, the expected performance can be expected to be even lower than the cold

environment experiment shown. The calculated daily power usage of 2.282 W from EQT 2, would more than likely be the maximum power usage over two days instead of one, to make the battery pack last for a period of 6 months.

Additionally, the battery pack subjected to a cold environment lasted longer than the battery pack tested in a warm (room temperature) environment, defying logic and therefore, should be repeated. This may have been a faulty battery pack or one which had been used previously and thus did not have its full charge.

4.6 Recommendations

The first recommendation would be to repeat the battery evaluation experiment in both a warm and cold temperature environment with new battery packs. By reiterating the experiment, results would be able to validated or disproven, and we would be able to understand why the warm environment battery cells did not perform as expected. This was not done in this project due to budget and time constraints.

Additionally, it is recommended these evaluation findings should be taken into consideration when determining the power usage schedule in the future.

5. Previous Power Board Evaluation

5.1 Introduction

It is important to evaluate the current version of the power management, monitoring and control system for the buoy, considering all design aspects. Additionally, as previously stated, it is assumed the power board is not working and thus, would require to be tested thoroughly.

The aim of this evaluation is to comprehensively understand and test the current power management, monitoring and control PCB board. This evaluation will then be used to inform the design of the next iteration of the board.

The power PCB board evaluated (Figure 30), was designed by Mr Justin Pead [40]. A full schematic of this design can be found in Appendix C.



Figure 30 - Original Power Board PCB

5.2 Breakdown and Understanding

The following modules make up the power management, monitoring and control PCB:

- Input control
- Current monitoring
- Regulator
- Soft start
- Capacitor bank
- I2C Isolation
- Microcontroller Unit
- IO peripherals
- Temperature
- Secondary Memory
- Ideal diode
- Current increaser
- Test points

Once an understanding of the above modules had been achieved, a set of tests were performed on the hardware to determine if it was working or not. This aided the next iteration of the design.

5.2.1 Input Control Module

The input control circuitry (Figure 31) serves the purpose of turning the circuit on or off via the use of an AO3401A P-Channel MOSFET. A reed switch and soldered jumper pad are connected in series to the gate of the MOSFET. If either of these break connection, the circuit would be powered on. The reed switch was used so a magnet could break the connection and turn the circuit on externally from the buoy casing. As a high current may be passing from the source to the drain of the MOSFET, two AO3401A P-Channel MOSFETs were used to distribute the load. Each MOSFET having a maximum current rating of 4 A [29] to give this circuit a rating of 8 A. A 1.65 MΩ resistor was used from the gate to ground (as not to have a floating voltage), but it also provides enough resistance to have minimal power loss through the resistors. The output of this module connects to the first current sensor.

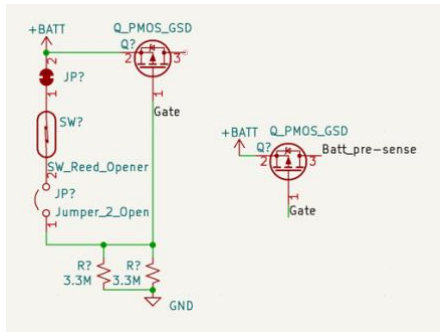


Figure 31 – Original Input Control Module [40]

5.2.2 Current Monitoring Module

The board uses two INA219 bi-directional power sensors. One is placed at the input to the circuit, after the input control module, and the other is positioned at the output of the circuit. This topology would allow the power usage of the load to be monitored. To calculate the power usage of the board, the power at the input is subtracted from the power at the output. The INA219s communicate with the microcontroller unit via an I²C protocol. The sensor addresses can be set by soldering the jumper pads connected to addresses A0 and A1 of the sensors. Figure 32 demonstrates the current monitoring module.

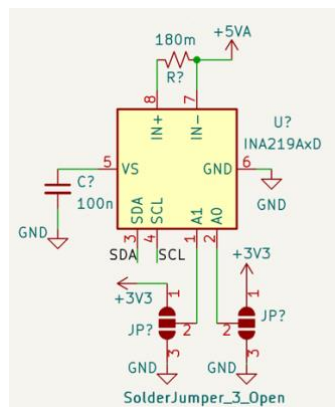


Figure 32 - Original Current Monitoring Module [40]

5.2.3 Regulator Module

MIC29302WU and TLV740P low-dropout linear voltage regulators were used to produce 5 V and 3.3 V, respectively. The input to the MIC29302WU comes from the output of the first INA219 sensor and connects to the input to the TLV740P. It is assumed to have been done to reduce the inefficiencies of the regulators. It is also assumed, the low-dropout regulators were chosen as the battery voltages are not significantly higher than the voltage that it is being regulated to. The MIC29302WU is a high-current, high-accuracy regulator [C11149] which is advantageous, as most of the higher current components (from the power budget) use 5 V. The designed original regulator module is seen in Figure 33.

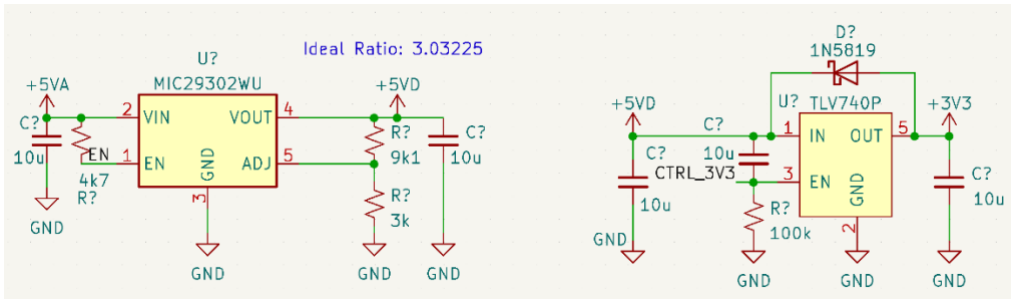


Figure 33 - Original Regulator Module [40]

5.2.4 Soft Start Module

The soft start module (Figure 34) is one of the more crucial parts of this system and is responsible for ensuring the current does not suddenly increase, but rather increases at a steadier rate. The module uses the SLVA156 design [38] but has been adapted in this version of the board to allow the soft start to reset via an external signal. This allows the microcontroller to control the current the load was able to draw in perpetuity, rather than it is working only on the start-up (as intended in the original SLVA156 design). The output of this soft start module connects directly to the capacitor bank. When the capacitor bank is not charged on start-up and is connected to power, it draws an extremely high current – highlighting the importance of this circuit. Because of this, an additional P-Chanell MOSFET is used to distribute the load. Additionally, an LED is placed between the input to the soft-start circuit and the capacitor bank thereby allowing a visual indicator of the charge of the capacitor bank without measuring the voltage. This module was meant to be able to limit the current below 1 A for a period of at least 1s [40].

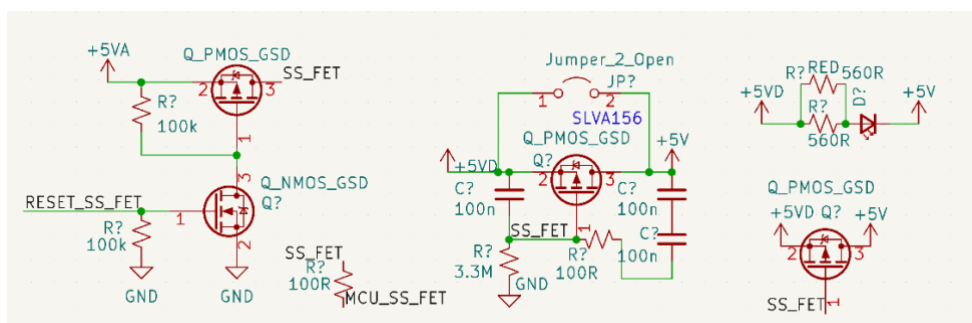


Figure 34 - Original Soft Start Module [40]

5.2.5 Capacitor Bank Module

The capacitor bank (Figure 35) consists of a 3 F electrolytic capacitor bank and a 2.1 mF ceramic capacitor bank, connected in series. It provides a large, stable amount of current quickly for shorter periods of time, in the event the battery pack is not able to provide this in a stable manner. The electrolytic capacitors act as the larger storage components but have a slower discharge due to their higher equivalent series resistance (ESR) [40]. Therefore, the smaller bank of ceramic capacitors which have a much lower ESR are added so that they can provide high-frequency bursts of current where needed [40].

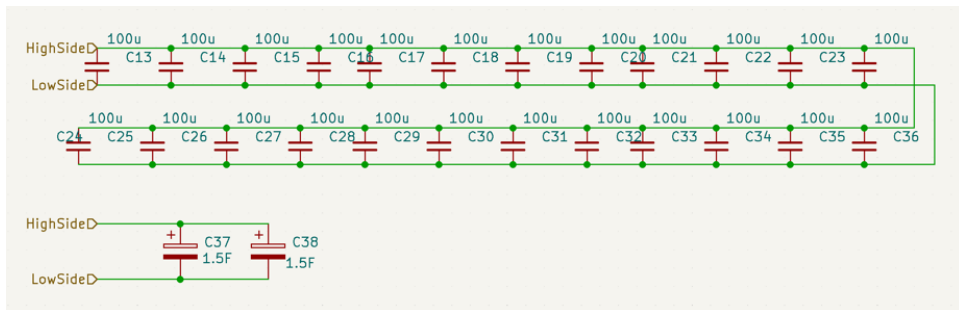


Figure 35 - Original Capacitor Bank Module [40]

5.2.6 I2C Isolation Module

Most communication via the board happens using the I2C communication protocol. The I2C isolation module (Figure 36) is responsible for determining if SDA and SCL signals from an external source, connect to the primary SDA and SCL lines on the board. This is important as it prohibits external I2C devices communicating with peripherals on the power board, if the main MCU is communicating with those peripherals. Consequently, the communication lines are used by devices that are meant to use them.

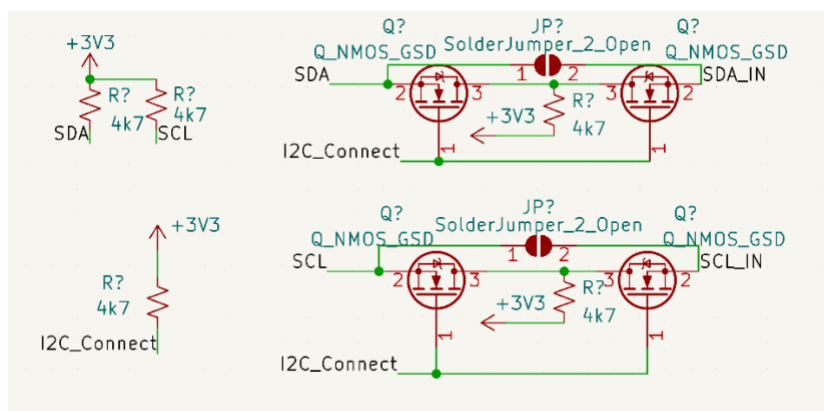


Figure 36 - Original I2C Isolation Module [40]

5.2.7 Microcontroller Unit Module

The microcontroller (Figure 37) makes use of the STM32G030F6 – a basic, low-power chip. It is responsible for all processing on the power board and connects to all the hardware peripherals.

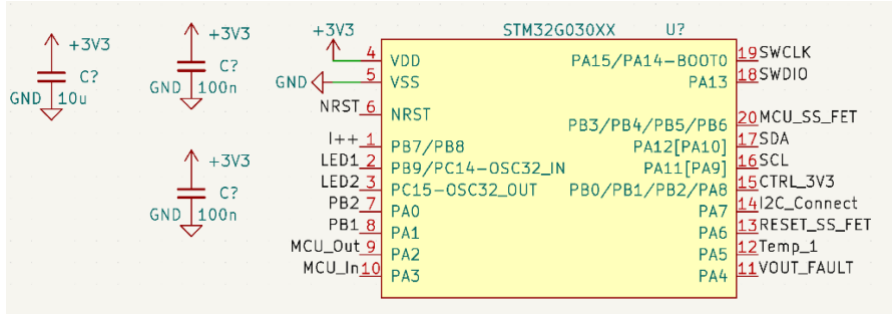


Figure 37 - Original Microcontroller Module [40]

5.2.8 IO Peripherals Module

The IO peripherals module (Figure 38) makes use of two push buttons and two LEDs. All 4 components connect to the microcontroller unit and, through software, can be used for a variety of purposes such as for debugging or feedback.

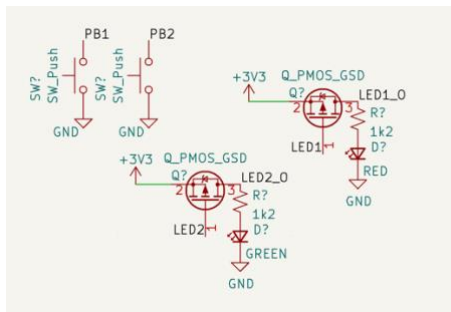


Figure 38 - Original IO Peripherals Module [40]

5.2.9 Temperature Module

The temperature module (Figure 39) uses a single TMP235A2 analogue temperature sensor.

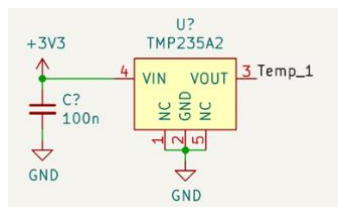


Figure 39 - Original Temperature Module [40]

5.2.10 Secondary Memory Module

The primary method of storing data is using the CAT24C256 EEPROM component. The soldered jumper pads allow the EEPROMs address to be set by the user. This is seen in Figure 40.

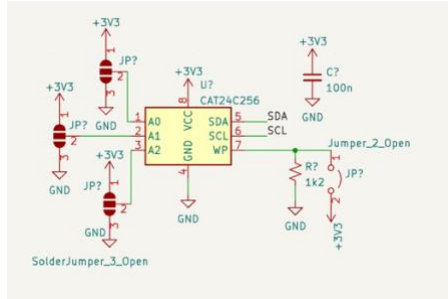


Figure 40 - Original Secondary Memory Module [40]

5.2.11 Current Increaser Module

If the batteries are not supplying enough current for the board or if the battery pack needs to be drained for a specific reason, the current increaser module (Figure 41) is a controllable method of increasing the current. This is achieved by having the regulated 5 V connected to a $560\ \Omega$ resistor and is controlled via a P-Channel MOSFET.

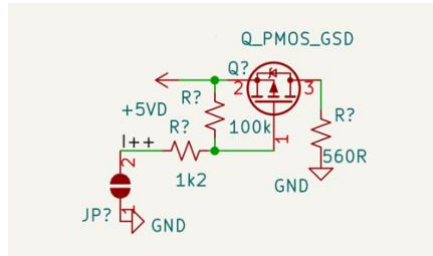


Figure 41 - Original Current Increaser Module [40]

5.2.12 Ideal Diode Module

The ideal diode module (Figure 42) allows an input of 3.3 V to power the board and thus will not allow 3.3 V to be used as an output. This acts as a form of protection so that the 3.3 V input pin can only provide 3.3 V, thereby stopping the power board from accidentally powering additional hardware which may be connected to the 3.3 V input pin.

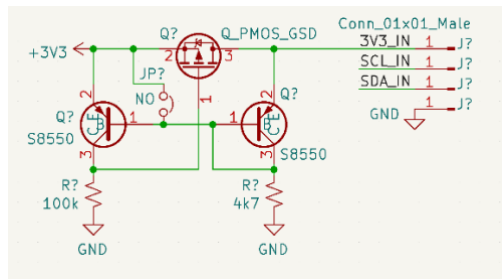


Figure 42 - Original Ideal Diode Module [40]

5.2.13 Test Points Module

The test points module is a set of soldered jumper pad test points that connect to many different points in the module to allow the user to assess those points.

5.3 Testing Methodology

The following test procedures were created to assess and evaluate the power management, monitoring and control board. It is important these tests are done in sequential order and the processes done by a previous test are left as is for the next test, unless otherwise stated.

5.3.1 Input Control Module

The input control module was analysed by connecting the power board to 7.2 V, supplied by a E3620A DC voltage generator. This mimics the voltage the battery would produce. Since the power board did not have a reed switch on it, two wires were connected to the solder pads and the solder pad jumper connection was soldered, to close the circuit. The expected output from the input control circuit, Batt_pre-sense, is expected to be 0 V in this state. Next, the mimic reed switch was opened by cutting the wire. The Batt_pre-sense voltage was then expected to be equal to input voltage of 7.2 V. These expected results are summarized in Table 9.

Component/State/Process	Expected Value
Reed switch - closed	0 V
Reed switch - open	7.2 V

Table 9 - Input Control Module Test Expectation

5.3.2 Regulator Module

With the voltage generator still supplying power, the regulators were examined by measuring the output voltage for each one. The expected output voltage for the MIC29302WU was 5.0 V and the expected voltage for the TLV740P was 3.3 V (Table 10). As the TLV740P required its enabled line to be on logic HIGH to switch on and regulate, and the microcontroller had not been programmed to output this logic HIGH to the regulator, a second voltage from the E3620A DC voltage generator was used to supply 3.3 V to the enable pin.

Component/State/Process	Expected Value
MIC29302WU	5.0 V
TLV740P	3.3 V

Table 10 - Regulator Module Test Expectation

5.3.3 Soft start

To test the soft start module the power supply was disconnected, and the capacitors were completely discharged. A KEYSIGHT DSO-X 2002A digital oscilloscope was then set up with two probes. Probe 1 was connected to the input to the soft start circuit and probe 2 was connected to the output. The oscilloscope would then trigger when probe 1 registered a voltage greater than 1 V; the power supply was connected, and the resulting waveform was captured. The time taken for the output voltage to equal the input voltage was measured. The RESET_SS_FET pin was then pulsed, and this was expected to restart the soft-start process. The soft start module test expectations are seen in Table 11.

Component/State/Process	Expected Value
Soft start time	1 s
SS_RESET_FET pulse resets soft start process	TRUE

Table 11 - Soft Start Module Test Expectation

5.3.4 I2C Isolation

The I2C isolation circuit was verified by ensuring the SDA and SCL signals matched signals on SDA_IN and SCL_IN, respectively, when the I2C_Connect was set to logic HIGH and that SDA and SCL signals did not have a signal. This was regardless of SDA_IN and SCL_IN, when the I2C_Connect was set to logic LOW. It was accomplished by using a Raspberry Pi Zero and connecting the Raspberry Pi's SDA and SCL pins to the SDA_IN and SCL_IN pins of the power board. The command ‘i2cdetect -y 1’ was run in a loop which would transmit and scan for the addresses of I2C devices via a I2C communication protocol. Probe 1 was connected to SDA of the power board and probe 2 was connected to SDA_IN of the power board. If I2C_Connect was set to logic HIGH, then both waveforms 1 and 2 should have matched. If I2C_Connect was set to logic LOW, then both waveforms 1 should have showed 0 V, regardless of what waveform 2 was performing. This method was repeated but moving the probes to SCL and SCL_IN, respectively. Table 12 demonstrates the expected values for the ISC Isolation module.

<u>Component/State/Process</u>	<u>Expected Value</u>
I2C_CONNECT LOW – SDA shows nothing	TRUE
I2C_CONNECT HIGH – SDA matches SDA_IN	TRUE
I2C_CONNECT LOW – SCL shows nothing	TRUE
I2C_CONNECT HIGH – SCL matches SCL_IN	TRUE

Table 12 - I2C Isolation Module Test Expectation

5.3.5 Ideal diode

To test the ideal diode module, the board was powered on and it was ensured the TLV740P regulator produced a voltage of 3.3 V. The 3V3_IN was measured using a Keysight U3401A digital multimeter and should read as 0 V. Next, a 3.3 V power source was connected to 3V3_IN. The 3.3 V test pad voltage was assessed and should read as 3.3 V. The power source to the board was disconnected and the 3.3 V test pad voltage was quantified and should read as 3.3 V. This is summarized in Table 13.

<u>Component/State/Process</u>	<u>Expected Value</u>
3V3_IN when board powered on	0 V
3.3 V test pad when board powered on and 3V3_IN is 3.3 V	3.3 V
3.3 V test pad when board powered off and 3V3_IN is 3.3 V	3.3 V

Table 13 - Ideal Diode Module Test Expectation

5.3.6 Microcontroller

The STM32G030F6 microcontroller was investigated by programming the microcontroller unit with a sample program. A MacBook Pro 2018 model computer was connected to the board via an STLink V3 and then the sample code from the STM32 Cube IDE application uploaded. The sample code was a program which set the CTRL_3V3 pin to logic HIGH and alternatively blinked the two LEDs from the IO Peripherals (Table 14). A link to this code can be found in Appendix D. This code should have uploaded and started running.

<u>Component/State/Process</u>	<u>Expected Value</u>
Sample code uploads and runs	TRUE

Table 14 – Microcontroller Unit Module Test Expectation

5.3.7 IO peripherals

The microcontroller test, when working, test the LEDs by causing them to blink. Each push button was also tested by placing the Keysight U3401A digital multimeter positive probe to the PB1 and PB2 test pads, along with a low voltage of 0.1 V. When the push buttons were not pushed, the multimeter read 0.1 V and when the buttons were pushed, the connection should be shorted, and the readings drop to 0 V (Table 15).

<u>Component/State/Process</u>	<u>Expected Value</u>
LED1 lights up	TRUE
LED2 lights up	TRUE
Push button 1 works	TRUE
Push button 2 works	TRUE

Table 15 - IO Peripheral Module Test Expectation

5.3.8 Capacitor bank

The capacitor bank was analysed by noting if it charges up to 5 V when the board was connected to power followed by investigating if it could provide current once the power supply was disconnected. This was accomplished by connecting the power supply to the board, charging the capacitor up to 5 V and using the multimeter to monitor the charging progress. The power supply was then disconnected, and the capacitors provided enough power to run the STM32G030F6 microcontroller with the sample code and flash the LED's on and off for a period of at least 1 minute (Table 16).

<u>Component/State/Process</u>	<u>Expected Value</u>
Capacitors charge	5 V
Capacitors are able to run microcontroller/LEDs for 1 minute	TRUE

Table 16 - Capacitor Bank Module Test Expectation

5.3.9 Temperature

The TMP235A2 analogue temperature sensor was examined by ensuring the output of the sensor was varying with a change in temperature. This was attained by ensuring the board was powered and measuring the output of the sensor using a digital multimeter. When a finger was placed on the sensor, the heat from the finger increases the temperature of the sensor and a change in the output voltage observed (Table 17).

<u>Component/State/Process</u>	<u>Expected Value</u>
TMP235A2 output voltage change with heat change	TRUE

Table 17 - Temperature Module Test Expectation

5.3.10 Current increaser

The current increaser module can be tested by setting the I++ test pad to logic LOW, which will then allow current to flow. This was verified by using the multimeter to ensure pin 3 of the P-channel MOSFET is 0 V when I++ is at logic HIGH and 5 V at logic LOW (Table 18).

<u>Component/State/Process</u>	<u>Expected Value</u>
I++ LOW, MOSFET drain	5 V
I++ HIGH, MOSFET drain	0 V

Table 18 - Current Increaser Module Test Expectation

5.3.11 Secondary Memory & Current Monitoring

The CAT24C256 EEPROM module and two INA219 current sensors were assessed by uploading a I2C address scanner program to the STM32G030F6 microcontroller. This would check if the devices could be recognized on the system and communicated with. Due to time constraints the program was not implemented, but Figure 43 exhibits the flow diagram of the code which would have been written.

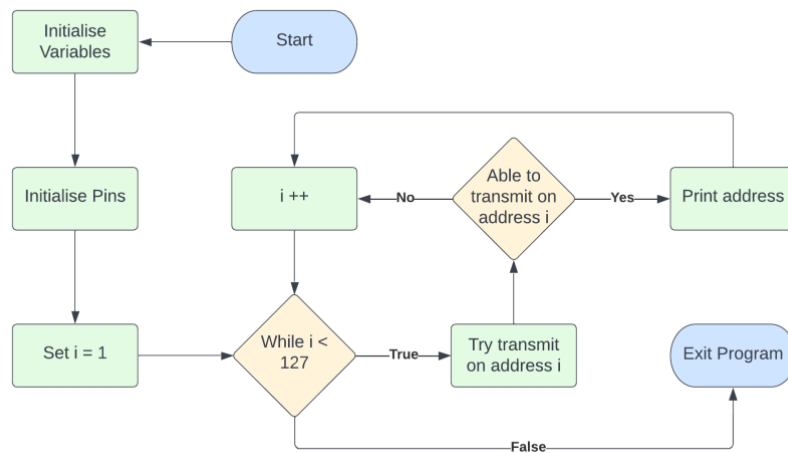


Figure 43 - I2C Scanner Flowchart

If all 3 devices were working and were configured correctly, their addresses would have been displayed (Table 19).

<u>Component/State/Process</u>	<u>Expected Value</u>
INA219 1 address displayed	TRUE
INA219 2 address displayed	TRUE
CAT24C256 address displayed	TRUE

Table 19 - Secondary Memory & Current Monitoring Modules Test Expectation

5.4 Results

The following section (Tables 20-29) outlines the results using the prior testing methodology described.

<u>Component/State/Process</u>	<u>Expected Value</u>	<u>Actual Value</u>
Reed switch - closed	0 V	0 V
Reed switch - open	7.2 V	7.28 V

Table 20 - Input Control Module Test Results

<u>Component/State/Process</u>	<u>Expected Value</u>	<u>Actual Value</u>
MIC29302WU	5.0 V	5.22 V
TLV740P	3.3 V	3.32 V

Table 21 - Regulator Module Test Results

<u>Component/State/Process</u>	<u>Expected Value</u>	<u>Actual Value</u>
Soft start time	1 s	8.6 ms
SS_RESET_FET pulse resets soft start process	TRUE	TRUE

Table 22 - Soft Start Module Test Results

<u>Component/State/Process</u>	<u>Expected Value</u>	<u>Actual Value</u>
I2C_CONNECT LOW – SDA shows nothing	TRUE	TRUE
I2C_CONNECT HIGH – SDA matches SDA_IN	TRUE	TRUE
I2C_CONNECT LOW – SCL shows nothing	TRUE	TRUE
I2C_CONNECT HIGH – SCL matches SCL_IN	TRUE	TRUE

Table 23 - I2C Isolation Module Test Results

<u>Component/State/Process</u>	<u>Expected Value</u>	<u>Actual Value</u>
3V3_IN when board powered on	0 V	0 V
3.3 V test pad when board powered on and 3V3_IN is 3.3 V	3.3 V	3.32 V
3.3 V test pad when board powered off and 3V3_IN is 3.3 V	3.3 V	3.29 V

Table 24 - Ideal Diode Module Test Results

<u>Component/State/Process</u>	<u>Expected Value</u>	<u>Actual Value</u>
Sample code uploads and runs	TRUE	TRUE

Table 25 – Microcontroller Unit Module Test Results

<u>Component/State/Process</u>	<u>Expected Value</u>	<u>Actual Value</u>
LED1 lights up	TRUE	TRUE
LED2 lights up	TRUE	TRUE
Push button 1 works	TRUE	TRUE
Push button 2 works	TRUE	TRUE

Table 26 - IO Peripheral Module Test Results

<u>Component/State/Process</u>	<u>Expected Value</u>	<u>Actual Value</u>
Capacitors charge	5 V	5.13 V
Capacitors are able to run microcontroller/LEDs for at least 1 minute	TRUE	TRUE

Table 27 - Capacitor Bank Module Test Results

<u>Component/State/Process</u>	<u>Expected Value</u>	<u>Actual Value</u>
TMP235A2 output voltage change with heat change	TRUE	TRUE

Table 28 - Temperature Module Test Results

<u>Component/State/Process</u>	<u>Expected Value</u>	<u>Actual Value</u>
I++ LOW, MOSFET drain	5 V	4.84 V
I++ HIGH, MOSFET drain	0 V	0 V

Table 29 - Current Increaser Module Test Results

5.5 Discussion

From the results of the tests done on the original power PCB board, many the modules passed the test procedures without any issues. The following modules passed the test procedures with no deviations from the expected results:

- Input control
- I2C Isolation
- Microcontroller
- IO peripherals
- Temperature
- Ideal diode
- Current increaser

Input control voltage however, had a slight deviation from the expected outcome yet this was due to the battery voltage being slightly higher than 7.2 V and was not a deviation from what was expected with regards to the input control module on the board.

The MIC29302WU regulator had an output voltage of 5.22 V which is higher than acceptable. It is also a linear voltage regulator which typically has much higher losses associated with them when compared to switching regulators. Therefore, it is recommended a buck regulator is used instead of the

MIC29302WU to get a more precise voltage with a higher conversion efficiency. The TLV740P regulated the voltage to 3.32 V which is within acceptable range from the desired 3.3 V. However, it is also a linear regulator and should be swapped out for a switching regulator in a future version of the board.

The soft start circuit only lasted 8.6 ms. This is shorter than the 1 second which was initially expected from the designer of the board [40]. Upon closer inspection of the SLVA156 datasheet [38] it can be seen this circuit uses a resistor value roughly 50 times greater as one of the example soft start circuit. This circuit had a soft start time of 10 ms before the voltage reached its maximum value. Therefore a start time of roughly 500 ms would have been expected. The next iteration of this board should have further investigation into the component values which make up this module and extent the soft start time. Although this is the case, the circuit modification which reset the soft start circuit worked accurately and efficiently. It is recommended for this to be utilized in the next iteration of the board.

The current increaser had a voltage 0.16 V lower than expected. This is more than adequate to increase the current draw from the batteries, and it is appropriate to take into the next iteration of the circuit without modification. The capacitor bank voltage was also higher than expected, however, this was more than likely due to the MIC29302WU regulator producing a higher voltage. It worked as expected in storing and releasing charge and kept the STM32G030F6 running the sample program for a few minutes. Consequently, the capacitor bank can also be taken onto the next iteration of the design without modification.

It should also be mentioned in this discussion that the board was not very user friendly. Namely the test pads on the back of the board were hard to use when wanting to see or test things on the front side of the board and there were no places to attach oscilloscope probes easily. A lot of soldering had to be done onto small test points to create wires to attach probes external wires too. Therefore, the next iteration of the design should look at a better way of utilising test points to make them more user friendly.

Additionally, the STM32G030F6 microcontroller needs to be programmed for the soft start to work initially. On the first start-up, when the microcontroller had not yet been programmed, the empty capacitors drew a very large current, and without the soft start being reset, it damaged some of the components. Therefore, it may be worthwhile looking into a method of disconnecting the capacitors until the STM32G030F6 has been programmed and is working correctly.

5.6 Conclusions

From the original board evaluation, several advantageous findings were made. The following modules were determined to work as expected, or to an acceptable level, and will go onto the next iteration without modification:

- Input control
- Capacitor bank
- I2C Isolation
- Microcontroller
- IO peripherals
- Temperature
- Ideal diode
- Current increaser
- Test points

The regulators and soft start had appropriate initial findings but will need to be further modified to work efficiently in the next iteration of the board. The following three requirements should be used in the design of the next board:

- Switching to switching buck regulators
- Increase the soft start time to at least 5s
- Add a switch that can disconnect the capacitors whilst the microcontroller is being programmed

5.7 Recommendations

Since the I2C scanner program was not implemented and run during this test phase, the CAT24C256 EEPROM and INA219s could not be tested. The first recommendation for the future would be to test these components on the board by implementing the I2C scanner code as shown by the flowchart in Figure 44.

The second recommendation would be for all the test points to be connected to header pins. This would be a much easier way to debug and test the circuit. The final execution of the board should not have these pins as they will add to the cost of the board, but during testing, they will be advantageous.

A third recommendation would be to add physical switches or connection points which could isolate the battery completely from the circuit. Even though the input control works effectively, it still draws a low current, and it would be better to have a way to manually disconnect the circuit, while everything is still assembled.

Additionally, it would be wise to change LED 1's colour from red to either yellow or blue. The soft start module makes use of a red LED already and the two LEDs could be confused with one another once power board is in a casing with the batteries. Therefore, it would be ideal to have different colours for different LEDs.

Finally, it was recommended on the schematic, to add a bootstrap capacitor to the enable line of the TLV740P 3.3 V regulator to allow it to regulate 3.3 V so that the STM32G030F6 microcontroller can turn on and manage the rest of the circuit [40].

6. New Power Board Design

6.1 Introduction

From the power budget, battery evaluation, and evaluation of the original board, the next design of the power management, monitoring and control board can be produced and implemented. Requirements from the above sections will be advantageous in guiding the design process and fixing the shortfalls of the previous design.

The following requirements were determined from Chapters 3 and 5 and state the new power management, monitoring and control PCB must:

- Be able to regulate the battery voltage to 3.3 V and 5 V
- Be able to suddenly increase current supply 470 mA
- Be able to handle a maximum current of 800 mA
- Make use of switching buck regulators
- Increase the soft start time to at least 5s
- Add a switch which can disconnect the capacitors whilst the microcontroller is being programmed

The primary focus of this iteration of the design will be (i) the addition of switching regulators, (ii) the addition of more physical switches, (iii) the addition of TX and RX lines to interface with the STMG030F6, and (iv) to make the board more user friendly and easier to test/debug.

A link to all the design files can be found in Appendix D.

6.2 Design Methodology

6.2.1 Previous Design

From the original power board evaluation, many of the modules passed the testing procedures and were deemed adequate to be used in this iteration of the design. The modules included:

- Input control
- Capacitor bank
- I2C Isolation
- Microcontroller
- IO peripherals
- Temperature
- Ideal diode
- Current increaser
- Test points

All these modules, except the input control module, ideal diode module and microcontroller module, were used in this iteration of the design. The design of these modules was created by Mr Justin Pead [40]. As these modules were covered in detail in Chapter 5, they will not be explained in detail in this section.

6.2.2 Regulation Module

The main upgrade to the new board was the use of buck converters (Figure 44). Both the 5 V regulator and 3.3 V regulator make use of the TPS62050DGS step-down converters. These regulators are variable output, high efficiency (up to 95%), low quiescent current, overcurrent protected switching regulators which can take in voltage ranges from 2.7 V to 10 V [41]. This makes them ideal for this application. Due to their variable output, the same package can be used for both the 5 V regulator and the 3.3 V regulator. The resistor, capacitor, inductor setups for regulating for the different voltages were duplicated from their corresponding component datasheets [41]. The output of the 5 V regulator connects into the input of the 3.3 V regulator to help further minimise losses.

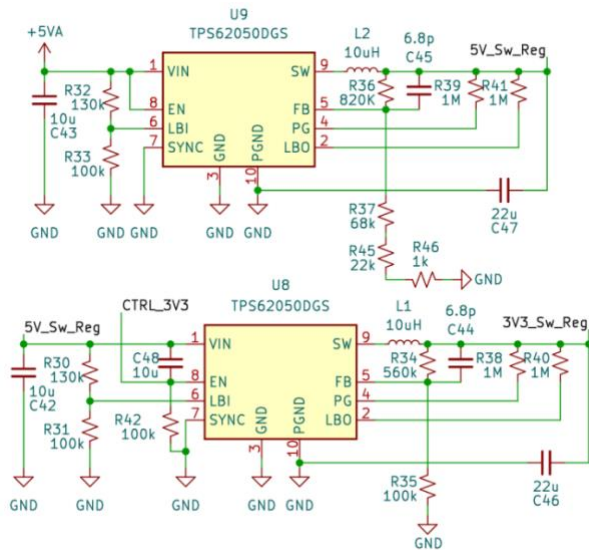


Figure 44 - Switching Regulator

Since this was a new method of regulating the voltage, it was uncertain how it would perform. Hence, the linear voltage regulators from the original board were added (Figure 45). The only upgrade made to this module was the addition of the bootstrap capacitor to the enable line of the TLV740P 3.3 V regulator so it would activate on start-up.

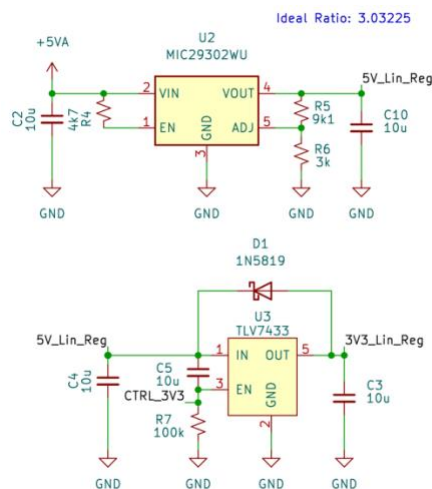


Figure 45 - Updated Linear Regulator

The regulator would be separated by a set of header pins and a jumper connector to bridge the gap from the regulator to the rest of the circuit was used (Figure 46). This allows the user to choose if they would like to use the switching or the linear regulators. When the STM32G030F6 microcontroller has not yet been programmed, the empty capacitors draw a very large current, and without the soft start being reset, it damaged components. Due to this, it may be worthwhile exploring a method of disconnecting the capacitors until the STM32G030F6 has been programmed and is functioning. This manual method whereby the user is able to remove the jumper connector and choose which regulator to use, acts as a switch and therefore concurrently resolving another issue.



Figure 46 - Regulator Type Connector

6.2.3 Soft Start Module

The soft start module in the original report was only limiting the current for 8.6 ms before it needed a reset. To rise this period, all capacitors in the soft start module were increased by a factor of 100 and replaced with 10 uF capacitors (Figure 47). This, in theory, should be sufficient to raise the soft start time period.

To verify this theory, the soft start circuit was implemented on a breadboard and was assessed using the same testing methodology as detailed under the Soft Start subheading in the Testing Methodology in Chapter 5. The larger value capacitors proved to work well as it allowed the soft start time to be increased to roughly 7s.

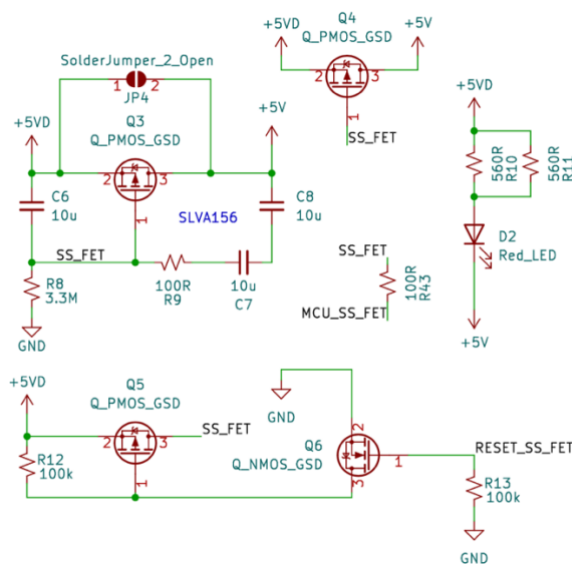


Figure 47 - Updated Soft Start Module

6.2.4 Test Points Module

The test points were upgraded by connecting them to header pins (Figure 48). This would allow for a more user-friendly experience when attempting to measure and use test points during the testing and debugging phase of the project. The soldered test pads were also maintained on the board as an additional option for the user.

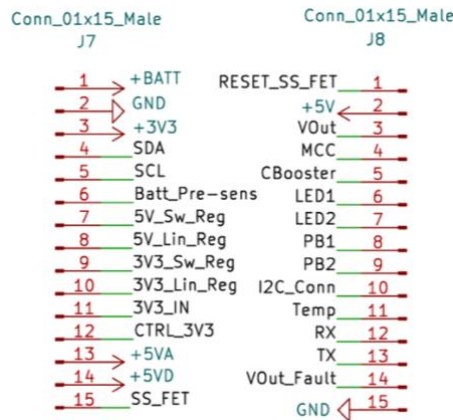


Figure 48 - Updated Test Points Pins

6.2.5 *Input Control Module*

The solder pad from the input of the control module was redundant and was not a dynamic method of monitoring the input control P-Channel MOSFET. Therefore, the solder jumper pad was replaced with two header pins which could be bridged using a jumper connector (Figure 49). This is a more dynamic and simpler method of controlling the MOSFET to turn on/off. A header pin connection was also used to break the circuit between the battery pack and the input to the input control module circuit. This would be bridged by a jumper connector and therefore provides the user a method of physically disconnecting the battery pack from the rest of the circuit.

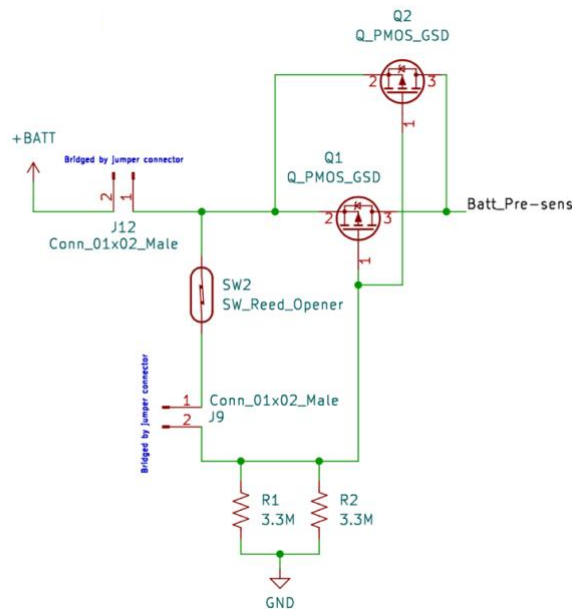


Figure 49 - Updated Input Control Module

6.2.6 Microcontroller Module

The microcontrollers module PA2 and PA3 pins were changed from MCU_IN and MCU_OUT to transmission and receiver pins, respectively (Figure 50). This new addition would allow the STM32G030F6 to utilise serial communication and thereby, could connect to a USB interface on a home computer system. It would be an advantageous way of getting data from the microcontroller sent to a display using a serial communication protocol.

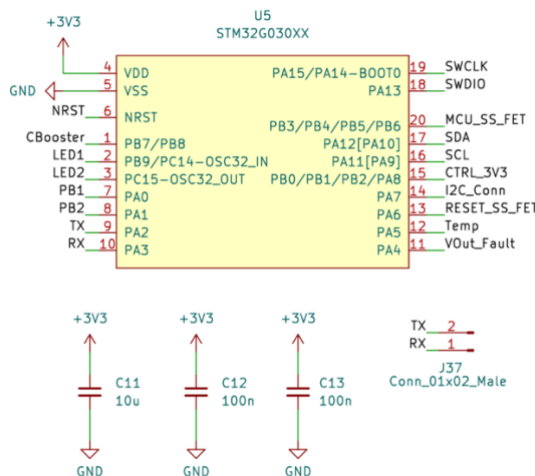


Figure 50 - Updated Microcontroller Unit

6.2.7 Additional Changes

The ideal diode module also received header pins on its input connections. The IO peripherals module had its red LED colour changed to blue, so that all the LEDs had a unique colour and would not be confused with one another.

6.2.8 *Implementation*

The design schematic was done using the KiCAD schematic editor. From there each component was assigned a footprint. This was then edited in the KiCAD PCB editor to create the layout for the final PCB design (Figure 51).

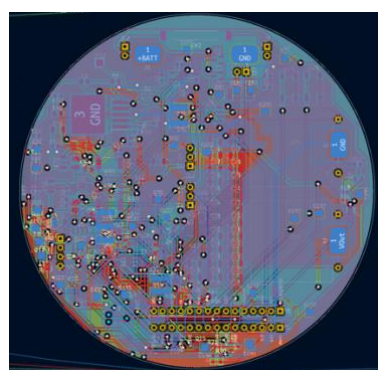


Figure 51 - KiCAD PCB Design

The design files were then sent to JCL PCB in Shenzhen, China for manufacturing before the PCB board was delivered back to UCT (Figure 52).



Figure 52 - Latest PCB Board

6.3 Testing Methodology

The following module test procedures were outlined in the Testing Methodology section in Chapter 5 and will be conducted as described in that section. These are outlined as follows:

- Soft start
- Capacitor bank
- I2C Isolation
- IO peripherals
- Temperature
- Secondary Memory
- Ideal diode
- Current increaser
- Current monitoring

6.3.1 Input Control Module

The input control module would be undergoing the same test as it did in Chapter 5, with the exception that it also had the jumper connector on the header pins to test, which allowed for options for control (Table 30). While one method of control was being tested, the other method of control was left alone and completed the circuit, thereby only changing one variable at a time.

Component/State/Process	Expected Value
Reed switch - closed	0 V
Reed switch - open	7.2 V
Jumper connection - closed	0 V
Jumper connection - open	7.2 V

Table 30 - Updated Input Control Module Test Expectation

6.3.2 Regulator Module

The regulator module had identical testing methodology as it did in Chapter 5, apart from having the TPS62050DGS switching regulators to test for (Table 31). The outputs of the linear and switching regulators were tested respectfully.

Component/State/Process	Expected Value
MIC29302WU	5.0 V
TLV740P	3.3 V
TPS62050DGS - 5.0 V	5.0 V
TPS62050DGS - 3.3 V	3.3 V

Table 31 – Updated Regulator Module Test Expectation

6.3.3 Microcontroller Module

The microcontroller module would follow consistent analysis techniques as did in the last evaluation with the exception the address to be printed would be sent via the new serial communication lines to see if they work as expected (Table 32).

Component/State/Process	Expected Value
Sample code uploads and runs	TRUE
Sends data via serial communication	TRUE

Table 32 - Updated Microcontroller Unit Module Test Expectation

6.3.4 Soft Start Module

The soft start module would follow the same assessment procedure as did in the last estimation with the exception that the soft start time must be at least 5s long as described by the requirements at the introduction of this Chapter 6 (Table 33).

Component/State/Process	Expected Value
Minimum soft start time	5 s
SS_RESET_FET pulse resets soft start process	TRUE

Table 33 - Soft Start Module Test Expectation

6.4 Results

Tables 34-44 outline the results using the above-mentioned testing methodology in Section 6.3.

Component/State/Process	Expected Value	Actual Value
Reed switch - closed	0 V	0
Reed switch - open	7.2 V	7.26 V
Jumper connection - closed	0 V	0 V
Jumper connection - open	7.2 V	7.26 V

Table 34 – New PCB Input Control Module Test Results

<u>Component/State/Process</u>	<u>Expected Value</u>	<u>Actual Value</u>
MIC29302WU	5.0 V	5.68 V
TLV740P	3.3 V	3.33 V
TPS62050DGS – 5.0 V	5.0 V	5.12 V
TPS62050DGS – 3.3 V	3.3 V	3.31 V

Table 35 - New PCB Regulator Module Test Results

<u>Component/State/Process</u>	<u>Expected Value</u>	<u>Actual Value</u>
Minimum soft start time	5 s	8.4 s
SS_RESET_FET pulse resets soft start process	TRUE	TRUE

Table 36 - New PCB Soft Start Module Test Results

<u>Component/State/Process</u>	<u>Expected Value</u>	<u>Actual Value</u>
I2C_CONNECT LOW – SDA shows nothing	TRUE	TRUE
I2C_CONNECT HIGH – SDA matches SDA_IN	TRUE	TRUE
I2C_CONNECT LOW – SCL shows nothing	TRUE	TRUE
I2C_CONNECT HIGH – SCL matches SCL_IN	TRUE	TRUE

Table 37 - New PCB I2C Isolation Module Test Results

<u>Component/State/Process</u>	<u>Expected Value</u>	<u>Actual Value</u>
3V3_IN when board powered on	0 V	0 V
3.3 V test pad when board powered on and 3V3_IN is 3.3 V	3.3 V	3.31 V
3.3 V test pad when board powered off and 3V3_IN is 3.3 V	3.3 V	3.30 V

Table 38 - New PCB Ideal Diode Module Test Results

<u>Component/State/Process</u>	<u>Expected Value</u>	<u>Actual Value</u>
Sample code uploads and runs	TRUE	FALSE
Sends data via serial communication	TRUE	FALSE

Table 39 - New PCB Microcontroller Unit Module Test Results

<u>Component/State/Process</u>	<u>Expected Value</u>	<u>Actual Value</u>
LED1 lights up	TRUE	TRUE
LED2 lights up	TRUE	TRUE
Push button 1 works	TRUE	TRUE
Push button 2 works	TRUE	TRUE

Table 40 - New PCB IO Peripheral Module Test Results

<u>Component/State/Process</u>	<u>Expected Value</u>	<u>Actual Value</u>
Capacitors charge	5 V	5.08 V
Capacitors are able to run microcontroller/LEDs for at least 1 minute	TRUE	FALSE

Table 41 - New PCB Capacitor Bank Module Test Results

<u>Component/State/Process</u>	<u>Expected Value</u>	<u>Actual Value</u>
TMP235A2 output voltage change with heat change	TRUE	TRUE

Table 42 - New PCB Temperature Module Test Results

<u>Component/State/Process</u>	<u>Expected Value</u>	<u>Actual Value</u>
I++ LOW, MOSFET drain	5 V	4.92 V
I++ HIGH, MOSFET drain	0 V	0 V

Table 43 - New PCB Current Increaser Module Test Results

<u>Component/State/Process</u>	<u>Expected Value</u>
INA219 1 address displayed	TRUE
INA219 2 address displayed	TRUE
CAT24C256 address displayed	TRUE

Table 44 – New PCB Secondary Memory & Current Monitoring Modules Test Expectation

6.5 Discussion

From the results of the tests done on the new power PCB board, many the modules passed the test procedures without any issues. The following modules passed the assessment processes without any divergence from the anticipated results:

- Input control
- Soft start
- I2C Isolation
- IO peripherals
- Temperature
- Ideal diode
- Current increaser

As previously found, the input control voltage had a slight deviation from the norm, but this was due to the battery voltage being higher than 7.2 V. This was still expected with regards to the input control module on the board.

The MIC29302WU regulator had a higher output voltage of 5.68 V which is unacceptably high. When comparing this result to the original PCB result, Table 21, this is significantly higher. Considering the regulators had the same arrangement, this is an abnormality which should be investigated further. The

TPS62050DGS switching regulators performed better than the MIC29302WU and TLV7433 regulators for controlling closer to 5.0 V and 3.3 V, respectively. The switching regulators will also make a positive difference in the power consumption of the board due to their higher efficiency.

The soft start circuit also exceeded expectations, lasting 8.4 seconds compared to the 8.6 ms of the previous iteration. It is interesting that the capacitors were increased by a factor of 100, but the increase in time was closer to a factor of 1000. This indicates the size of the capacitor is related to the soft start time non-linearly.

The results highlighted the microcontroller did not work. The STM32 Cube IDE application kept giving a “no device found” error on upload. Upon closer investigation, it was seen there was an error made in the new schematic – the NSRT, GND, SWDIO, SWCLK programming lines had got mixed up making it impossible to program the microcontroller. This is a vital flaw which will need to be fixed in the next iteration. Unfortunately, this also made the current monitoring module and secondary memory module test impossible. It also affected the capacitor test, as the capacitor was not able to perform its second part of the test due to the STM32G030F6 not being programmed. This kept the enable line for the voltage regulators high. As the capacitors were still charged up, and although not tested, there is no indication which proves the capacitors would not hold and release that charge as done so on the original board.

The new blue LED colour worked well as to differentiate the LED colours apart. One big difference in testing and using this new board was the header pins. It made the debugging experience much easier and was a lot quicker to test as wires as it didn’t need to be soldered onto the test pads. The jumper connectors also worked efficiently as physical connection points which could be placed on and off the respective pins as needed.

6.6 Conclusions

From the original board evaluation a number of advantageous findings were made. The following modules were determined to work as expected and can be kept as is in a future update:

- Input control
- Soft start
- I2C Isolation
- IO peripherals
- Temperature
- Ideal diode
- Current increaser

The switching regulators worked effectively, but an investigation will need to be done to see as to why the MIC29302WU regulator was so unlike the voltage it should be producing. Many tests were unable to be done due to the programming pin error. The new header pins and minor changes around the board made a positive impact on the usability of the board.

6.7 Recommendations

The first thing which should be done is fixing the programming pin mix-up error. This would be crucial in allowing the board to function properly and would allow the remainder of the tests to be concluded. It is also recommended the MIC29302WU regulator is investigated further, as to why it was not

producing the 5V it should be. It would also be advantageous to have a comprehensive in depth test to compare the linear regulators to the switching regulators for the applications it will be experiencing.

Additionally, it would be ideal to see an in-depth program be developed for the board, so that it can start to be tested for the extreme conditions it will be experiencing. A program that logs data from sensors, similar to the Raspberry Pi datalogger from Chapter 4 would be good place to start. Further recommendations on implementing a software program for the board, would be to have the current sensors trigger an interrupt to pulse the RESET_SS_FET pin if the current exceeds a limit of 600 mA. This would ensue that the soft start is then always reset when the current exceeds a safe operating limit and manages the current to lower levels.

Another recommendation would be to rearrange the PCB design. The current board makes use of 4 layers, but it is possible to get it down to 2 layers. This will end up making the board more cost effective.

7. Conclusion

The main aim of this project was to create a power monitoring and control system which can be implemented in the UCT SHARC ice-tethered buoy. This procedure will provide power to all the other subsystems on the buoy, which are integral to collecting in situ measurements from the area it is deployed in. The system will need to deal with a variety of operating modes, variations in loads and changes in efficiency due to the extreme weather. To assess these components, the (i) battery performance was evaluated, (ii) the previous power board was reviewed and (iii) the new power board design was analysed.

After the battery performance tests had been concluded, three main findings were believed. The power board must be able to (i) regulate the battery voltage to 3.3 V and 5 V, (ii) suddenly increase current supply 470 mA and (iii) handle a maximum current of 800 mA. The major recommendation suggested was to bring the power budget forward by creating a day-to-day schedule of which of the components mentioned in the power budget's methodology subchapter are in (i) what process state, (ii) when they are in that process state, and (iii) when they change from that state. This will allow for the power budget to be utilised more effectively in predicting how much power would be used, when it would be used, and could allow for optimising of the schedule as to maximise efficiency.

Additionally, the battery evaluation experiment was deemed to be successful, as the hardware performed as expected and valuable data was gathered from the experimentation. This is due to the battery packs performing more poorly than what they were rated to do and as real-time measurements in colder temperatures than -20 °C are expected for the SHARC buoy, even lower performance should be anticipated. As the cold temperature test battery had a longer lifespan than the warm temperature one, it is assumed this may have been due to a faulty battery pack or one which did not have its full charge. This experiment will need to be repeated.

Next, the previous power board was assessed based on the current version of the power management, monitoring and control system for the buoy, thereby considering all design aspects of it. 9 modules were deemed to work either to an acceptable level or as expected, thereby their usage in the new power board design. These included the input control, capacitor bank, I2C isolation, microcontroller, IO peripherals, temperature, ideal diode, current increaser, and test points. The main changes made to the board were using switching regulators, increasing the soft start time to 5 s, and adding a switch which can disconnect the capacitors whilst the microcontroller is being programmed. Header pins, physical switches/connection points, LED 1's colour change, and the addition of a bootstrap capacitor were also recommended for the next iteration of the board.

These recommendations and changes from the power budget, battery evaluation, and evaluation of the original board were included in the next design of the power management, monitoring and control board. Seven modules including the input control, soft start, I2C isolation, IO peripherals, temperature, ideal diode, and current increaser were deemed to work as expected and recommended to be used in future iterations of the board. Unfortunately, due to human error, a programming pin mix-up error was made. Because of this mistake, many tests were not completed, and it would be recommended to rectify this mistake prior to future assessments. The MIC29302WU regulator also was not functioning correctly, yet the new header pins and minor changes around the board made a positive impact on the usability of the board. The final and main recommendation, would be to rearrange the PCB design from four layers down to two, consequently making the board more cost effective.

Overall, the project can be considered a success. A robust process of budgeting for power usage, power source evaluation, previous board evaluation, and new design methodologies were conducted. Reliable tests revealed expected results as well as some which need to be rectified or repeated, but thought-out recommendations have been made for future iterations of the board. An effective power management system was thoroughly tested and described, and the power PCB improved upon. Hopefully this power board will be used in future SHARC buoy expeditions.

8. List of References

- [1] "Antarctic Sea Ice", *Epa.gov*, 2022. [Online]. Available: https://www.epa.gov/sites/default/files/2021-04/documents/antarctic-sea-ice_documentation.pdf.
- [2] "WMO verifies one temperature record for Antarctic continent and rejects another", *World Meteorological Organization*, 2021. [Online]. Available: <https://public.wmo.int/en/media/press-release/wmo-verifies-one-temperature-record-antarctic-continent-and-rejects-another>.
- [3] M. Altawee, "The Use of Gravimetry Satellites for Measuring Ice and Sea Level Change", *GIS Lounge*, 2020. [Online]. Available: <https://www.gislounge.com/the-use-of-gravimetry-satellites-for-measuring-ice-and-sea-level-change/>.
- [4] J. C. Barnett, A. D. Rogers, G. Serafini, and J. R. Davies, "RISING GROUNDWATER LEVELS ASSOCIATED WITH SEA LEVEL RISE," *JDA Hydro*, Mar-2015. [Online]. Available: http://www.jdahydro.com.au/images/publications/Rising_Groundwater_Levels_Associated_with_Sea_Level_Rise.pdf.
- [5] C. Donlon, B. Berruti, A. Buongiorno, M.-H. Ferreira, P. Féménias, J. Frerick, P. Goryl, U. Klein, H. Laur, C. Mavrocordatos, J. Nieke, H. Rebhan, B. Seitz, J. Stroede, and R. Sciarra, "The Global Monitoring for Environment and Security (GMES) sentinel-3 mission," *Remote Sensing of Environment*, 28-Feb-2012. [Online]. Available: https://www.sciencedirect.com/science/article/pii/S0034425712000685?casa_token=5Fh7g7FgsoYAAAAA%3AMd5R3g_zzOkIKSdGfuacIb8Pf1FNBPc9AVfbIYqlAdK2aTXRhdWee2ezQhC1u2oQmNrz-gWIjOs.
- [6] M. Song, J. Y. Yang-Scharlotta, M. Ashtijou, and M. Mojarradi, "Evaluation of commercial-off-the-shelf (COTS) electronics for Extreme Cold Environments," *IEEE Xplore*, 2018. [Online]. Available: <https://ieeexplore.ieee.org/abstract/document/8396695>.
- [7] P. Gloersen, T. T. Wilheit, T. C. Chang, W. Nordberg, and W. J. Campbell, "Microwave Maps of the Polar Ice of the Earth," *JSTOR*, vol. 55, no. 12, pp. 1442–1448, Dec. 1974.
- [8] E. G. Njoku, J. M. Stacey, and F. T. Barath, "The Seasat Scanning Multichannel Microwave Radiometer (SMMR): Instrument description and performance," *IEEE Xplore*, Apr-1980. [Online]. Available: <https://ieeexplore.ieee.org/document/1145458>.
- [9] P. Gloersen and F. Barath, "A Scanning Multichannel Microwave Radiometer for Nimbus-G and seasat-A," *IEEE Xplore*, Apr-1997. [Online]. Available: https://ieeexplore.ieee.org/abstract/document/1145331?casa_token=QxFDLNeUEBoAAAAA%3A4zE5NE LH1GdBdQjVQmOzk7Qo5vKBQatK9NCO2OVH7zRjNU13gAc9GZiQbGyPiXBcjg04XhotEA.
- [10] F. J. Wentz, A well-calibrated ocean algorithm for special sensor microwave / imager, Apr-1997. [Online]. Available: <https://agupubs.onlinelibrary.wiley.com/doi/abs/10.1029/96JC01751>.
- [11] D. B. Kunkee, G. A. Poe, D. J. Boucher, S. D. Swadley, Y. Hong, J. E. Wessel, and E. A. Uliana, "Design and evaluation of the first special sensor microwave imager/sounder," *IEEE Xplore*, Mar-2008. [Online]. Available: https://ieeexplore.ieee.org/abstract/document/4475705?casa_token=MJ18sphn-n8AAAAA%3AM688UNqDHkpsNDlqjyhsaTuUWIGrJydzVLPUwr2xcYp_0493OAGvhfjHR1nIKcO70lyMNXAWZw.

- [12] D. B. Kunkee, S. D. Swadley, G. A. Poe, Y. Hong, and M. F. Werner, "Special Sensor Microwave Imager Sounder (SSMIS) radiometric calibration anomalies-part I: Identification and characterization," IEEE Xplore, Mar-2008. [Online]. Available: https://ieeexplore.ieee.org/abstract/document/4475707?casa_token=ek1SZYjCCMgAAAAA%3AFXFpqUr1tCQVZi6qFVy_98asKLZvNeNuv8IU2sJXAMcc6nkPBpBV0cOVOmZTy7yHHzbASAGw.
- [13] N. C. Grody, Classification of snow cover and precipitation using the special sensor microwave imager, Apr-1991. [Online]. Available: <https://agupubs.onlinelibrary.wiley.com/doi/abs/10.1029/91JD00045>.
- [14] C. A. Mears, D. K. Smith, and F. J. Wentz, Comparison of Special Sensor Microwave Imager and buoy-measured wind speeds from 1987 to 1997, Jun-2001. [Online]. Available: <https://agupubs.onlinelibrary.wiley.com/doi/abs/10.1029/1999JC000097>.
- [15] "Monitoring polar ice melting by combining data from different satellites", *Spie.org*, 2022. [Online]. Available: <https://spie.org/news/monitoring-polar-ice-melting-by-combining-data-from-different-satellites?SSO=1>.
- [16] S. W. Laxon, K. A. Giles, A. L. Ridout, D. J. Wingham, R. Willat, R. Cullen, R. Kwok, A. Schweiger, J. Zhang, C. Haas, and S. Hendricks, CryoSat-2 estimates of Arctic sea ice thickness and volume, Jan-2013. [Online]. Available: <https://agupubs.onlinelibrary.wiley.com/doi/full/10.1002/grl.50193>.
- [17] M. McMillan, A. Shepherd, A. Sundal, K. Briggs, A. Muir, A. Ridout, A. Hogg, and A. Wingham, "Increased ice losses from Antarctica detected by Cryosat-2," Increased ice losses from Antarctica detected by CryoSat-2, May-2014. [Online]. Available: <https://agupubs.onlinelibrary.wiley.com/doi/full/10.1002/2014GL060111>
- [18] S. Clerc, C. Donlon, F. Borde, N. Lamquin, S. E. Hunt, D. Smith, M. McMillan, J. Mittaz, E. Woolliams, M. Hammond, C. Banks, T. Moreau, B. Picard, M. Raynal, P. Rieu, and A. Guérou, "Benefits and lessons learned from the sentinel-3 tandem phase," MDPI, 19-Aug-2020. [Online]. Available: <https://www.mdpi.com/2072-4292/12/17/2668>.
- [19] IMBIE Team, "Mass balance of the Antarctic Ice Sheet from 1992 to 2017," Nature News, 13-Jun-2018. [Online]. Available: <https://www.nature.com/articles/s41586-018-0179-y>.
- [20] I. Aslamov, G. Kirillin, M. Makarov, K. Kucher, R. Gnatovsky, and N. Granin, "Autonomous System for Lake Ice Monitoring," MDPI, 20-Dec-2021. [Online]. Available: <https://www.mdpi.com/1424-8220/21/24/8505/htm>.
- [21] J. Whitlock, "Autonomous Sea Ice Measurements for the Changing Arctic", ProQuest, 2018. [Online]. Available: <https://www.proquest.com/openview/8c38ad40c8e6d7e4e76bf318f64340b3/1.pdf?pq-origsite=gscholar&cbl=18750>.
- [22] J. Rabault, G. Sutherland, O. Gundersen, A. Jensen, A. Marchenko and Ø. Breivik, "An open source, versatile, affordable waves in ice instrument for scientific measurements in the Polar Regions", Science Direct, 2022. [Online]. Available: <https://www.sciencedirect.com/science/article/abs/pii/S0165232X19300230>.
- [23] D. Langis, P. Stabeno, C. Meinig, C. Mordy, S. Bell and H. Tabisola, "Low-Cost Expendable Buoys for Under Ice Data Collection", IEEE Xplore, 2022. [Online]. Available: https://www.researchgate.net/publication/330300648_Low-Cost_Expendable_Buoys_for_Under_Ice_Data_Collection.

- [24] M. E. Tobin, "Sun, Sea, and Ice: Autonomous observations of sea ice mass balance and the partitioning of solar radiation in Arctic sea ice," Dartmouth College, 2020. [Online]. Available: <https://digitalcommons.dartmouth.edu/cgi/viewcontent.cgi?article=1015&context=engs88>.
- [25] Energizer Brands, "Alkaline Manganese Dioxide", *Data.energizer.com*, 2018. [Online]. Available: https://data.energizer.com/pdfs/alkaline_appman.pdf.
- [26] D. Langis, P. J. Stabeno, C. Meinig, C. W. Mordy, S. W. Bell, and H. M. Tabisola, "Low-cost expendable buoys for under Ice Data Collection," IEEE Xplore, Oct-2018. [Online]. Available: https://ieeexplore.ieee.org/abstract/document/8604752?casa_token=_4d8jXTak6IAAAA%3AgnUI957MQYFpNZyWa-t9Yz8JVsmNIFmW-GvGDEGVK-wxrAq9juprKNR5vTCiXvm62mu_eNjyxw.
- [27] J. N. Jacobson, "SHARC BUOY: Robust firmware design for a novel, low-cost autonomous platform for the Antarctic Marginal Ice Zone in the Southern Ocean," OpenUCT Home, 2021. [Online]. Available: <https://open.uct.ac.za/handle/11427/35788>.
- [28] A. Hassan, Y. Savaria, and M. Sawan, "Electronics and packaging intended for emerging harsh environment applications: A Review," IEEE Xplore, Oct-2018. [Online]. Available: <https://ieeexplore.ieee.org/abstract/document/8370238>.
- [29] F. R. Ihmig, S. G. Shirley, and H. Zimmermann, "Batch screening of commercial serial flash-memory integrated circuits for low-temperature applications," Cryogenics, 23-May-2015. [Online]. Available: <https://reader.elsevier.com/reader/sd/pii/S0011227515000648?token=4887926BF4CBD0AC4BC1C615C317C9CFEEFD23C918A533B518B7F860DE3E15603A057EAB160D1621DE4B824F90n.d.DEC&originRegion=eu-west-1&originCreation=20221106164430>.
- [30] R. L. Patterson, A. Hammoud, and M. Elbuluk, "Electronic components for use in extreme temperature aerospace applications - NASA technical reports server (NTRS)," NASA, Feb-2008. [Online]. Available: <https://ntrs.nasa.gov/citations/20090004677>.
- [31] H. Hanamura, T. Masuhara, O. Minato, Y. Sakai, and T. Hayashida, "Operation of bulk CMOS devices at very low temperatures," IEEE Xplore, Jun-1986. [Online]. Available: <https://ieeexplore.ieee.org/document/1052555>.
- [32] K. Marasco, "How to successfully apply low dropout regulators - eeweb," AN-1072 Application Notes, 2010. [Online]. Available: <https://www.eeweb.com/wp-content/uploads/articles-app-notes-files-how-to-successfully-apply-low-dropout-regulators-1495439389.pdf>.
- [33] H. J. Zhang, "<https://www.analog.com/media/en/technical-documentation/app-notes/an140.pdf>," Analogue Devices, Oct-2013. [Online]. Available: <https://www.analog.com/media/en/technical-documentation/app-notes/an140.pdf>.
- [34] X. Li, X. Cheng, H. Zhang, J. Zhang, F. Hui, and F. Wang, "A multi-interface ice and snow remote monitoring platform in the Polar Region," IEEE Xplore, Nov-2014. [Online]. Available: https://ieeexplore.ieee.org/abstract/document/6755469?casa_token=fsXWLFTjN7kAAAAA%3AYRSGUKuy8a48io1q1m9buEeo5spq0ZjpBP_MSQCliaX11qurxpQZConxlabovFBc00Ddg7fy3Q.
- [35] J Jaguemont, L. Boulon, and Y. Dubé, "A comprehensive review of lithium-ion batteries used in hybrid and electric vehicles at cold temperatures," Applied Energy, 17-Dec-2015. [Online]. Available: <https://www.sciencedirect.com/science/article/abs/pii/S0306261915014841>.
- [36] T. Instruments, "Monotonic, inrush current limited start-up for linear regulators," SLVA156 . [Online]. Available: <https://www.ti.com/lit/an/slva156/slva156.pdf>.

[37] J. A. De Lima and W. Pimenta, "An accurate sense-fet current limiter with embedded softstart for Linear DC/DC converters," IEEE Xplore, May-2011. [Online]. Available: <https://ieeexplore.ieee.org/abstract/document/5938121>.

[39] B. Adey, "Buoy Energy Budget Manual," thesis, 2021.

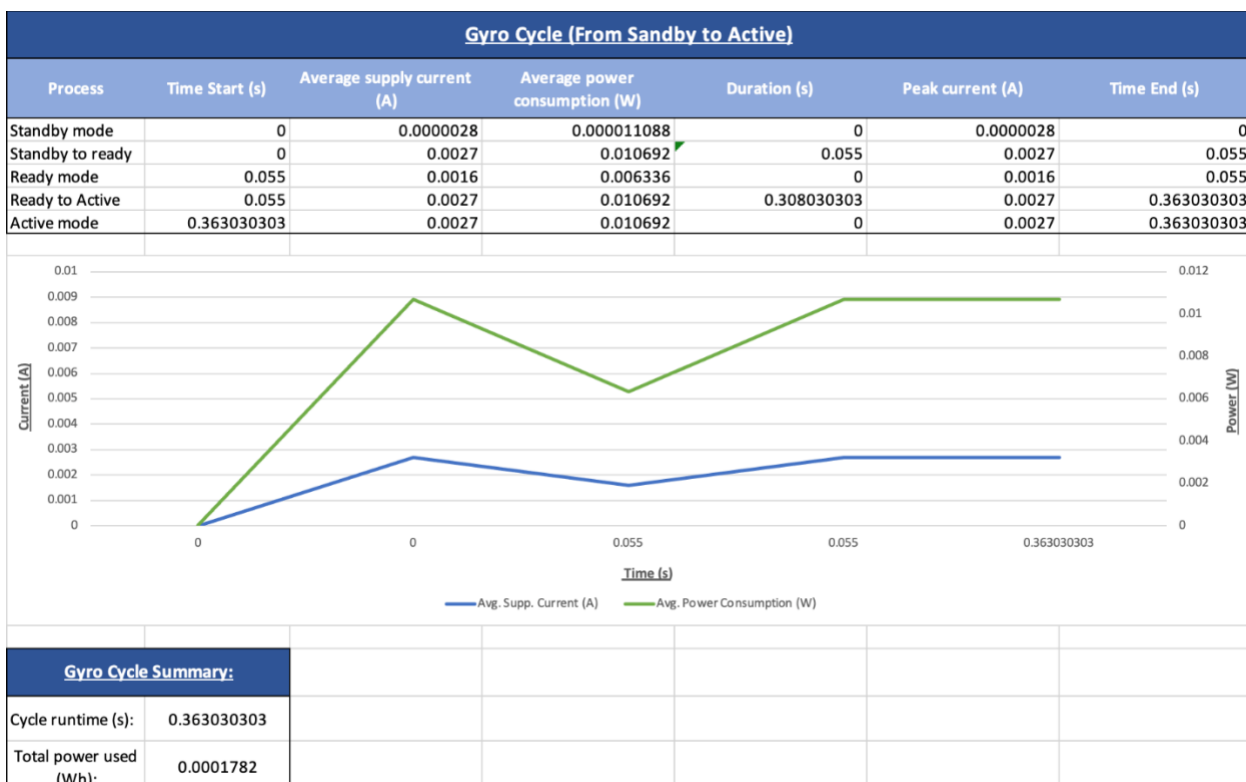
[40] J. Pead, 2022. EEE Department/University of Cape Town

[41] T. Instruments, "TPS6205X 800-mA synchronous step-down converter datasheet (rev. F) - ti.com," Jul-15AD. [Online]. Available: <https://www.ti.com/lit/ds/symlink/tps62050.pdf>. [Accessed: 01-Nov-2022].

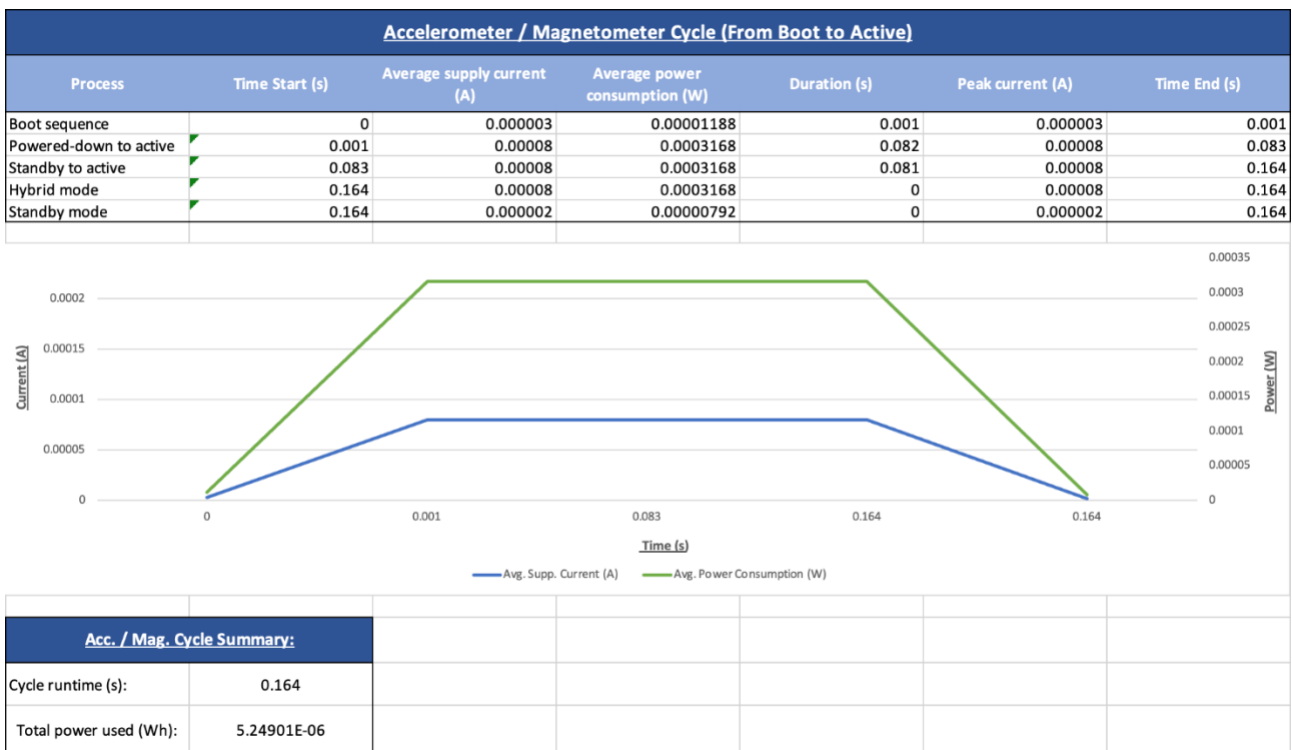
9. Appendix A

Full power budget spreadsheet:

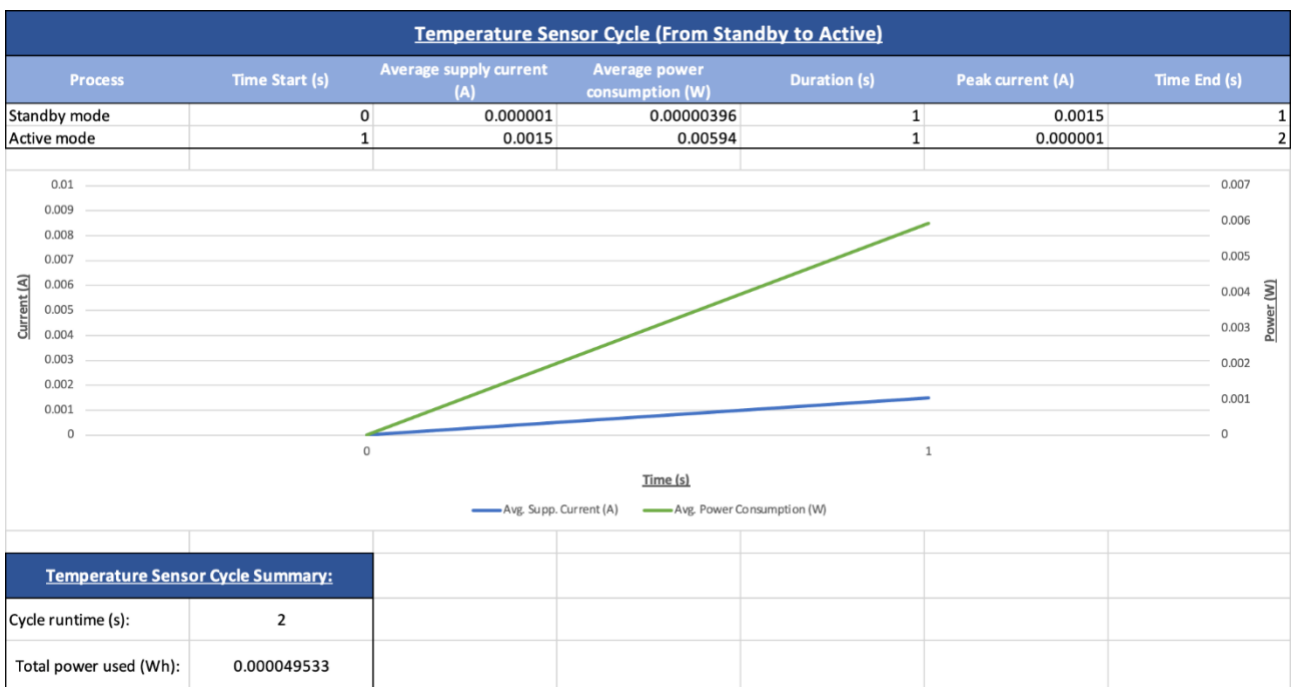
Gyro						
Notes						
FXAS21002						
Power consumption						
Process	Description	Average supply current (A)	Average power consumption (W)	Duration (s)	Peak current (A)	Runtime (s)
Active mode	Active	0.0027	0.010692	0	0.0027	
Ready mode	Ready	0.0016	0.006336	0	0.0016	
Standby mode	Standby	0.0000028	0.000011088	0	0.0000028	
Ready to Active	Transition from Ready mode to Active mode	0.0027	0.010692	0.308030303	0.0027	
Standby to Active	Transition from Standby mode to Active mode	0.0027	0.010692	0.363030303	0.0027	



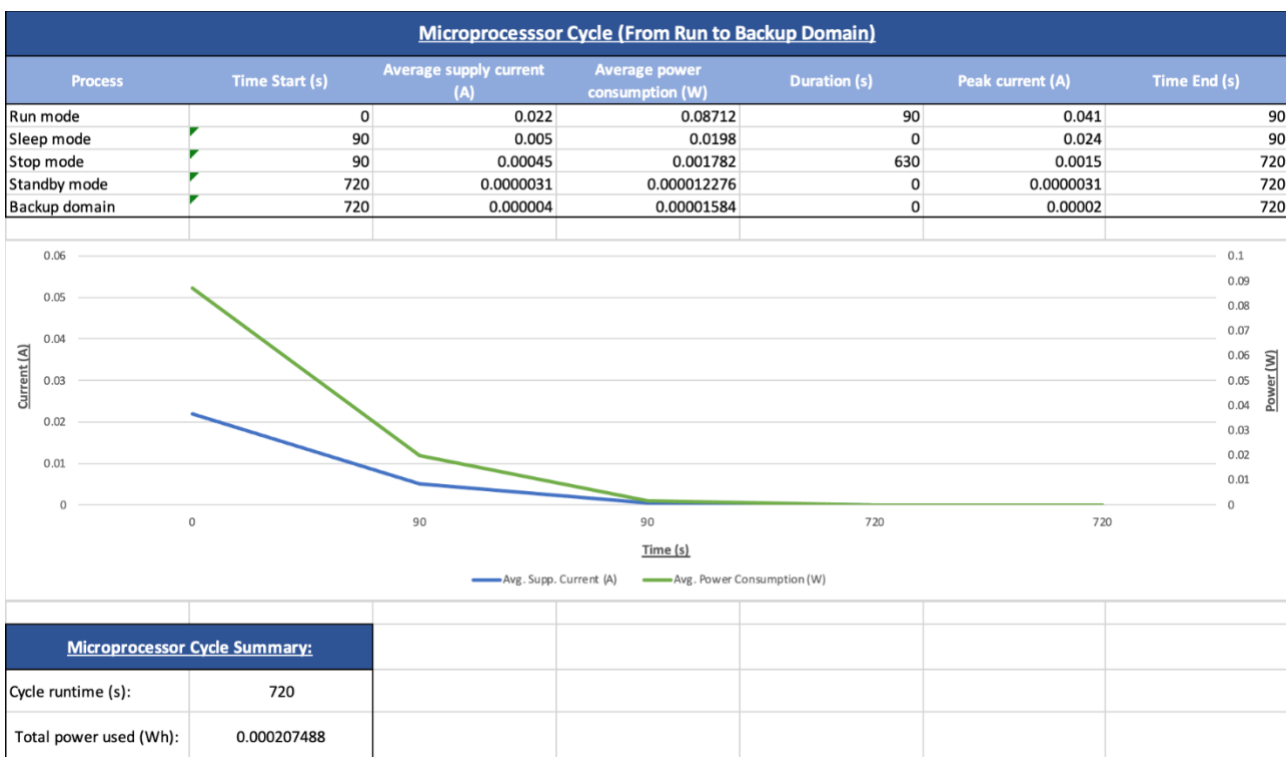
Accelerometer / Magnetometer						
Notes						
FXOS8700						
Parameters						
Voltage supply						
ODR (Hz)						
Power consumption						
Process	Description	Average supply current (A)	Average power consumption (W)	Duration (s)	Peak current (A)	Notes
Boot sequence	Boot sequence	0.000003	0.00001188	0.001	0.000003	
Powered-down to active	Time to obtain valid data from power-down mode to active mode	0.000008	0.0003168	0.082	0.000008	
Standby to active	Time to obtain valid data from standby mode to active mode	0.000008	0.0003168	0.081	0.000008	
Hybrid mode	Hybrid (ODR = 25 Hz)	0.000008	0.0003168	0	0.000008	
Standby mode	Standby @ 25°C	0.000002	0.000000792	0	0.000002	



Temperature Sensor							
Notes							
DS18B20							
Parameters							
Voltage supply							
Power consumption							
Process	Description	Average supply current (A)	Average power consumption (W)	Duration (s)	Peak current (A)	Notes	
Active Mode	Supply current during active	0.0015	0.00594	1	0.0015		
Standby mode	Standby	0.000001	0.00000396	1	0.000001		

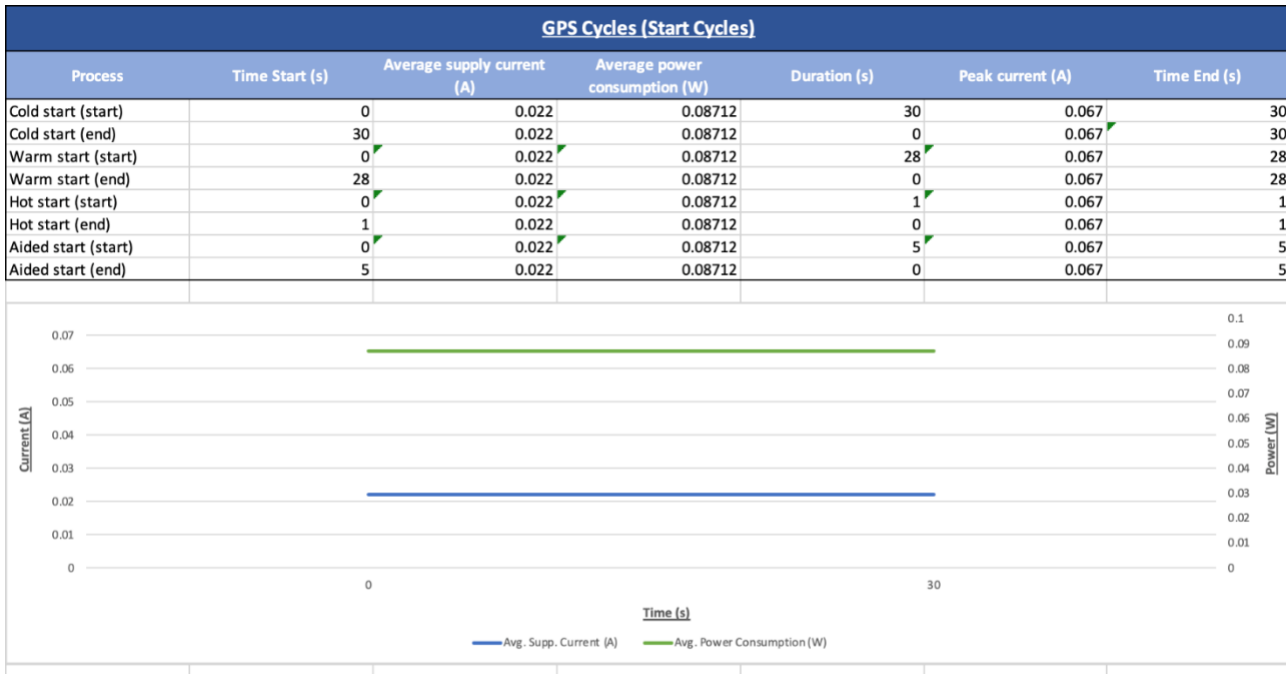


Microcontroller						
Notes						
STMF405QD						
Running at 60 MHz, all peripherals disabled Assuming ART Accelerator disabled						
Parameters						
Voltage supply		3.3				
Power consumption						
Process	Description	Average supply current (A)	Average power consumption (W)	Duration (s)	Peak current (A)	Notes
Run mode	Run	0.022	0.08712	90	0.041	
Sleep mode	Sleep	0.005	0.0198	0	0.024	
Stop mode	Stop	0.00045	0.001782	630	0.0015	
Standby mode	Standby	0.0000031	0.000012276	0	0.0000031	
Backup domain	Backup domain	0.000004	0.00001584	0	0.00002	



GPS						
Notes						
NEO-7M-0-000						
Parameters						
Voltage supply						
Power consumption						
Process	Description	Average supply current (A)	Average power consumption (W)	Duration (s)	Peak current (A)	Notes
Cold start	Acquisition	0.022	0.08712	30	0.067	
Warm start	Acquisition	0.022	0.08712	28	0.067	
Hot start	Acquisition	0.022	0.08712	1	0.067	
Aided start	Acquisition	0.022	0.08712	5	0.067	
Tracking continuous	Tracking (continuous mode)	0.017	0.06732	0	0.067	
Tracking power save	Tracking (power save mode / 1 Hz)	0.005	0.0198	0	0.067	
Powered down	turned off	0	0	0	0	*error* no standby mode specified on datasheet

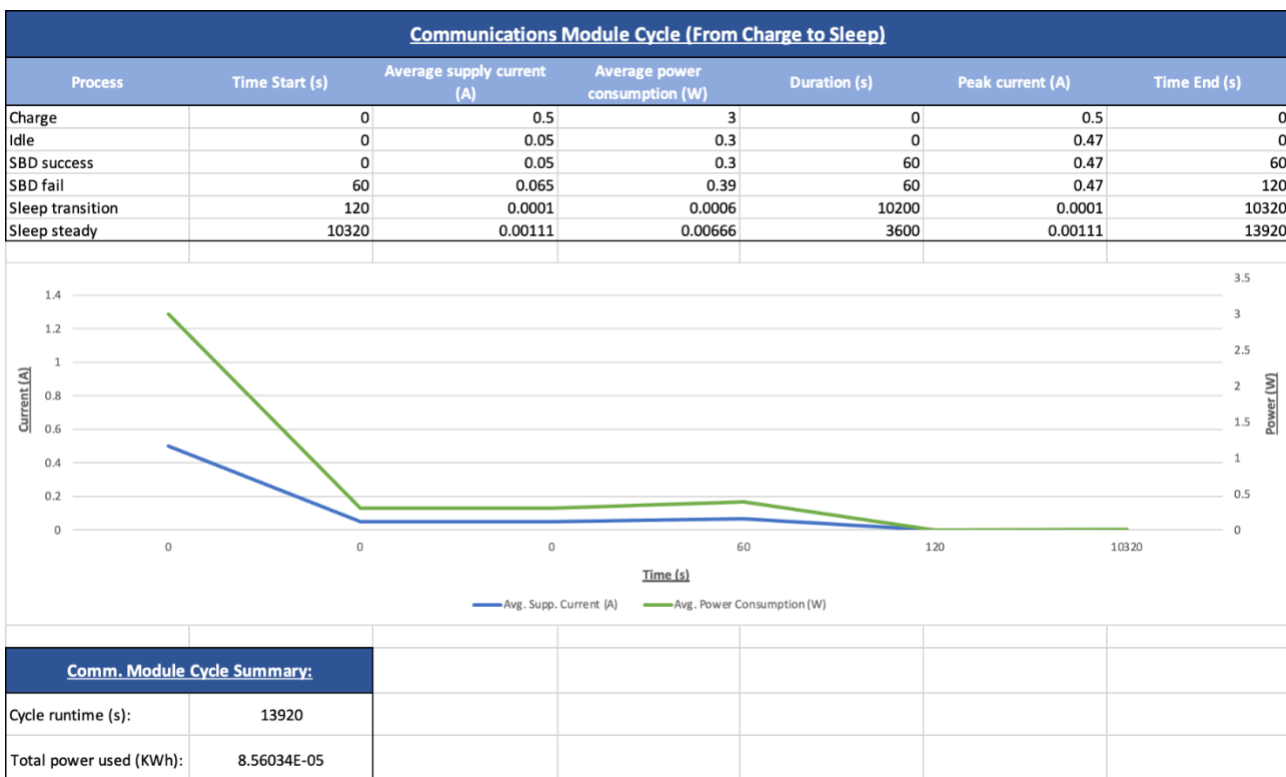
GPS Cycles (Start Cycles)						
Process	Time Start (s)	Average supply current (A)	Average power consumption (W)	Duration (s)	Peak current (A)	Time End (s)
Cold start (start)	0	0.022	0.08712	30	0.067	30
Cold start (end)	30	0.022	0.08712	0	0.067	30
Warm start (start)	0	0.022	0.08712	28	0.067	28
Warm start (end)	28	0.022	0.08712	0	0.067	28
Hot start (start)	0	0.022	0.08712	1	0.067	1
Hot start (end)	1	0.022	0.08712	0	0.067	1
Aided start (start)	0	0.022	0.08712	5	0.067	5
Aided start (end)	5	0.022	0.08712	0	0.067	5



The graph displays the power consumption and current over time. The blue line represents the average supply current (A), which is constant at 0.022 A from 0 to 30 seconds. The green line represents the average power consumption (W), which is constant at 0.08712 W from 0 to 30 seconds.

GPS Cycle Summary:	
Cycle runtime (s):	30
Total power used (Wh):	0.001452

Communications Module											
Notes											
RockBLOCK 9603d											
Parameters											
Voltage supply											
Power consumption											
Process	Description	Average supply current (A)	Average power consumption (W)	Duration (s)	Peak current (A)	Notes					
Charge	Charging	0.5	3	0	0.5	When the device is first powered or after a long period of disuse (typically more than a week)					
Idle	Idle	0.05	0.3	0	0.47	Powered-up, but not executing any commands.					
SBD success	Active mode - Successful SBD transmission	0.05	0.3	60	0.47						
SBD fail	Active mode - Failed SBD transmission	0.065	0.39	60	0.47						
Sleep steady	Average current after 1 hour in sleep mode	0.0001	0.0006	10200	0.0001	*error* peak current not given					
Sleep transition	Average current during first hour in sleep mode after active mode	0.00111	0.00666	3600	0.00111	*error* peak current not given					



10. Appendix B

Battery evaluation datalogger code:

```
#Author: Benjamin Connolly
#Date: 04/10/2022
#Project: SHARC Buoy - Data logger

#imports
import time
import board
import os
import adafruit_dht
import RPi.GPIO as GPIO
from ina219 import INA219
from ina219 import DeviceRangeError
from datetime import datetime
from getkey import getkey
from sys import exit

#Reading INA219 data
def readINA(SHUNT_OHMS, MAX_EXPECTED_AMPS):
    ina1 = INA219(SHUNT_OHMS, MAX_EXPECTED_AMPS, address=0x40)
    ina1.configure(ina1.RANGE_16V)
    ina2 = INA219(SHUNT_OHMS, MAX_EXPECTED_AMPS, address=0x41)
    ina2.configure(ina2.RANGE_16V)

    ina1.wake()
    ina2.wake()
```

```
return data

#Main code
if __name__ == "__main__":
    print("Executing code...")
    print("Setting up...")

#Initial setup
DHT = adafruit_dht.DHT22(board.D4)
temperature = DHT.temperature
humidity = DHT.humidity

SHUNT_OHMS = 0.1
MAX_EXPECTED_AMPS = 0.7

LED1_PIN = 22
LED2_PIN = 23
LED3_PIN = 24
RELAY_PIN = 5
BUZZER_PIN = 6
CONTROL_PIN = 18

GPIO.setwarnings(False)
GPIO.setmode(GPIO.BCM)

GPIO.setup(LED1_PIN, GPIO.OUT)
GPIO.setup(LED2_PIN, GPIO.OUT)
GPIO.setup(LED3_PIN, GPIO.OUT)
```

```

#Creating CSV data log file

f = open("data.csv", "a")

f.write(str(datetime.now()) + "\n")

f.write("Time(s),Humidity(%),Temperature(C),")

f.write("Voltage1(V),Current1(mA),Power1(mW),ShuntVoltage1(mV),")

f.write("Voltage2(V),Current2(mA),Power2(mW),ShuntVoltage2(mV)\n")

f.close()

print("Logging data...")

while True:

    #Reading environmental data

    try:

        temperature = DHT.temperature

        humidity = DHT.humidity

        print(temperature)

        print(humidity)

        data = dict()

        data[0] = round(humidity, 3)

        data[1] = round(temperature, 3)

        break

    except RuntimeError as error:

        print(error.args[0])

        time.sleep(0.1)

        continue

```

```

        elif round(data[1]) == 350:
            GPIO.output(LED1_PIN, GPIO.LOW)
            GPIO.output(LED2_PIN, GPIO.HIGH)
            GPIO.output(LED3_PIN, GPIO.LOW)

        elif data[1] >= 350:
            GPIO.output(LED1_PIN, GPIO.LOW)
            GPIO.output(LED2_PIN, GPIO.LOW)
            GPIO.output(LED3_PIN, GPIO.HIGH)
            dc -= 0.01

        if data[1] >= 700:
            GPIO.output(RELAY_PIN, GPIO.LOW)
            GPIO.output(BUZZER_PIN, GPIO.HIGH)
            print("limits exceeded - shutting down experiment...")
            break

#Ensuring that the suty cycle is kept between 0 and 100
if dc > 100:
    dc = 100

elif dc < 0:
    dc = 0

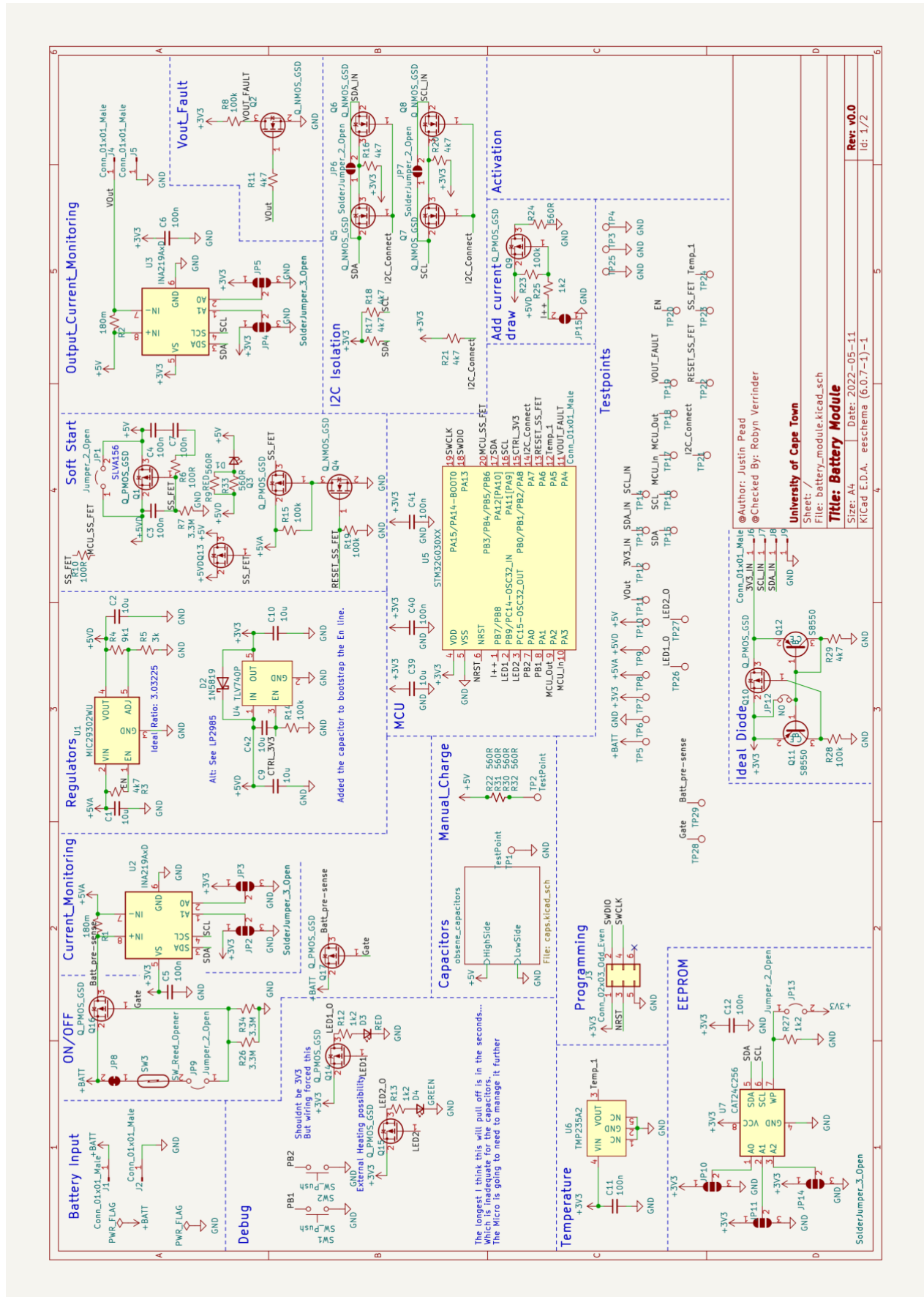
CONTOL_PWM.ChangeDutyCycle(dc)

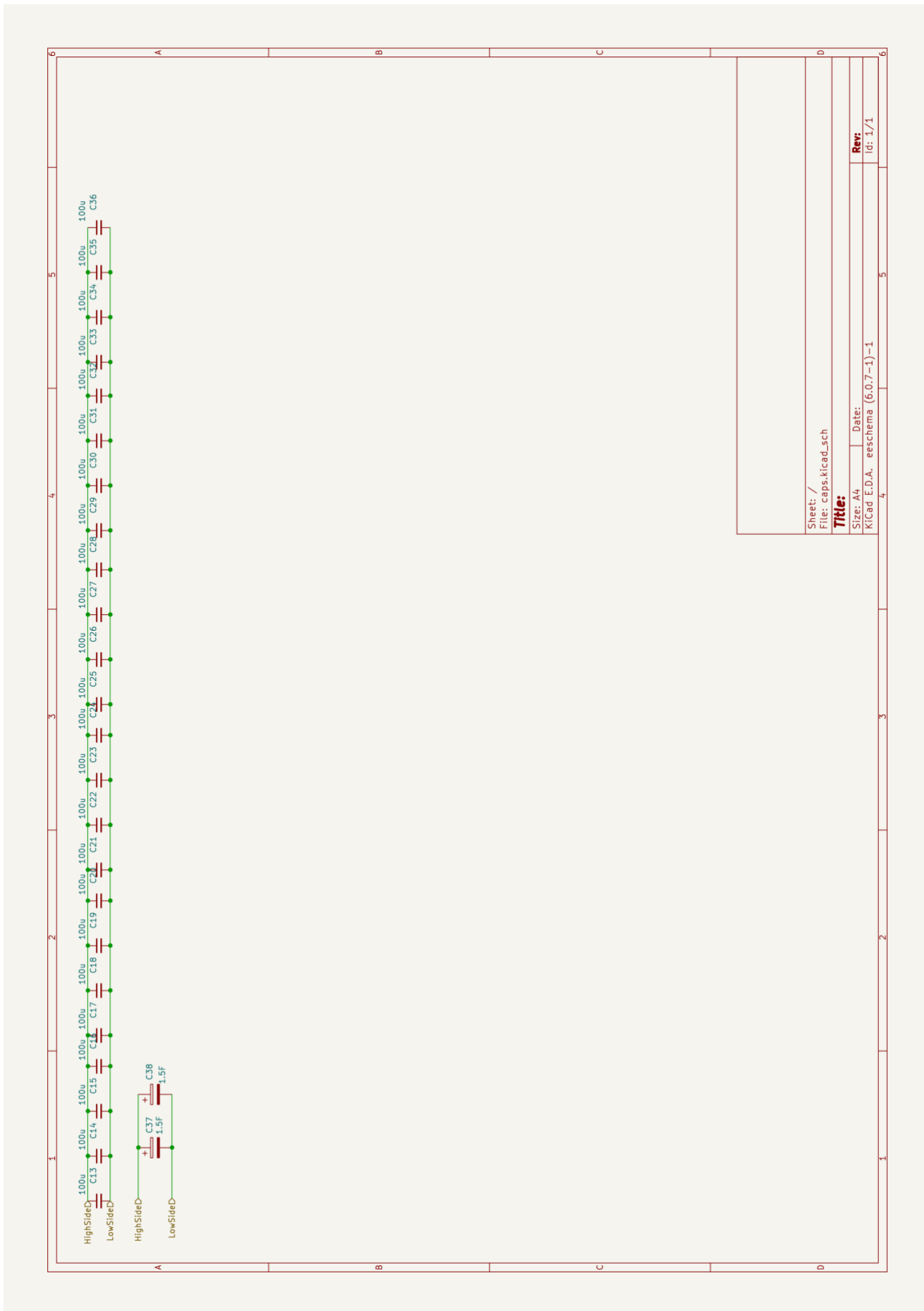
#Logging data every 10 seconds

```

```
#Printing values to the terminal  
  
os.system('clear')  
  
print("Voltage: ", data[0])  
  
print("Current: ", data[1])  
  
print("Power: ", data[2])  
  
print("S-Voltage: ", data[3])  
  
print("Duty-cycle: ", dc)  
  
print()  
  
  
#Giving a slight delay to allow all processes to run  
  
time.sleep(0.2)  
  
  
#Exiting the program if ^C is pressed  
  
except KeyboardInterrupt:  
  
    GPIO.cleanup()  
  
    print("Exited.")
```

11. Appendix C





12. Appendix D

The following link leads to the GITHUB repository for this project:

<https://github.com/cnnben002/SHARC-Buoy-Power-Module>

13. EBE Faculty: Assessment of Ethics in Research Projects

Application for Approval of Ethics in Research (EiR) Projects
Faculty of Engineering and the Built Environment, University of Cape Town

ETHICS APPLICATION FORM

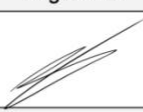
Please Note:

Any person planning to undertake research in the Faculty of Engineering and the Built Environment (EBE) at the University of Cape Town is required to complete this form **before** collecting or analysing data. The objective of submitting this application *prior* to embarking on research is to ensure that the highest ethical standards in research, conducted under the auspices of the EBE Faculty, are met. Please ensure that you have read, and understood the **EBE Ethics in Research Handbook** (available from the UCT EBE, Research Ethics website) prior to completing this application form: <http://www.ebe.uct.ac.za/ebe/research/ethics1>

APPLICANT'S DETAILS			
Name of principal researcher, student or external applicant		Benjamin Connolly	
Department		EEE	
Preferred email address of applicant:		cnnben002@myuct.ac.za	
If Student	Your Degree: e.g., MSc, PhD, etc.	Undergraduate	
	Credit Value of Research: e.g., 60/120/180/360 etc.	40	
	Name of Supervisor (if supervised):	Robyn Verrinder	
If this is a researchcontract, indicate the source of funding/sponsorship		N/A	
Project Title		SHARC Buoy: Power Management and Control	

I hereby undertake to carry out my research in such a way that:

- there is no apparent legal objection to the nature or the method of research; and
- the research will not compromise staff or students or the other responsibilities of the University;
- the stated objective will be achieved, and the findings will have a high degree of validity;
- limitations and alternative interpretations will be considered;
- the findings could be subject to peer review and publicly available; and
- I will comply with the conventions of copyright and avoid any practice that would constitute plagiarism.

APPLICATION BY	Full name	Signature	Date
Principal Researcher/ Student/External applicant	Benjamin Connolly		17/08/2022
SUPPORTED BY	Full name	Signature	Date
Supervisor (where applicable)	Robyn Verrinder		17/08/2022

APPROVED BY	Full name	Signature	Date
HOD (or delegated nominee) Final authority for all applicants who have answered NO to all questions in Section 1; and for all Undergraduate research (Including Honours).			
Chair: Faculty EIR Committee For applicants other than undergraduate students who have answered YES to any of the questions in Section 1.			